

Spring 3-2015

Aircraft De-Icing System Using Thermal Conductive Fibers

Min Soon Park
Embry-Riddle Aeronautical University

Follow this and additional works at: <https://commons.erau.edu/edt>



Part of the [Aeronautical Vehicles Commons](#)

Scholarly Commons Citation

Park, Min Soon, "Aircraft De-Icing System Using Thermal Conductive Fibers" (2015). *Doctoral Dissertations and Master's Theses*. 276.

<https://commons.erau.edu/edt/276>

This Thesis - Open Access is brought to you for free and open access by Scholarly Commons. It has been accepted for inclusion in Doctoral Dissertations and Master's Theses by an authorized administrator of Scholarly Commons. For more information, please contact commons@erau.edu.

AIRCRAFT DE-ICING SYSTEM USING THERMAL CONDUCTIVE FIBERS

A Thesis

Submitted to the Faculty

of

Embry-Riddle Aeronautical University

by

Min Soon Park

In Partial Fulfillment of the

Requirements for the Degree

of

Master of Science in Aerospace Engineering

March 2015

Embry-Riddle Aeronautical University

Daytona Beach, Florida

Aircraft De-Icing System Using Thermal Conductive Fibers

By

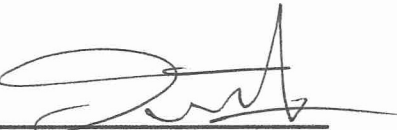
Min Soon Park

A Thesis prepared under the direction of the candidate's committee chairman, Dr. Daewon Kim, Department of Aerospace Engineering, and has been approved by the members of the thesis committee. It was submitted to the School of Graduate Studies and Research and was accepted in partial fulfillment of the requirements for the degree of Master of Science in Aerospace Engineering.

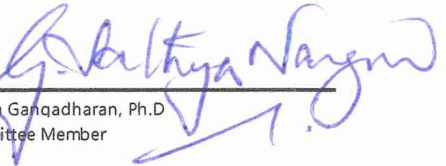
Thesis Review Committee

X 

Daewon Kim, Ph.D
Committee Chair

X 

Sirish Namilae, Ph.D
Committee Member

X 

Sathya Ganqadharan, Ph.D
Committee Member

X 

Yi Zhao, Ph.D
Graduate Program Coordinator

4/16/2015


Date

X 

Maj Mirmirani, Ph.D
Dean of College of Engineering

4/16/15

Date

X 

Robert Oxley, Ph.D
Associate Vice President of Academics

4-17-15

Date

Acknowledgements

I would like to dedicate this thesis to my family. Firstly, I would like to thank my parents, Jong Ki Park and Ae Ja Kim, for all their support and encouragement with love throughout my study at Embry-Riddle Aeronautical University.

I would like to thank my advisor, Dr. Daewon Kim. His guidance and confidence in my ability helped me successfully complete my thesis.

I would like to thank my committee members Dr. Sathya Gangadharan and Dr. Sirish Namilae, for taking time out of their busy schedule, and spending precious time to review my thesis.

I would like to offer my special thanks Mr. Michael Potash for helping me by making a temperature sensing equipment for my experimental setup.

I would also like to thank Stacey Junkins, an administrative assistant to the Aerospace Engineering Department. She was always kind enough to help and always greeted me with a bright smile.

Lastly, I would like to thank all the people who have believed in me and supported with all their hearts.

Abstract

Researcher: Min Soon Park

Title: Aircraft De-Icing System Using Thermal Conductive Fibers

Institution: Embry-Riddle Aeronautical University

Degree: Master of Science in Aerospace Engineering

Year: 2015

The accumulation of ice on the leading edges of aircraft wing poses complications for flight control as drag is increased with a tendency for higher relative turbulence over the wing. Pre-emptive and reactive ice removal techniques have been employed in the past by electromechanical, thermal, chemical and pneumatic methods. In this thesis, a carbon fiber fabric is utilized as a heating de-icer for composites aircraft wing surface structures. Two prototypes are constructed, tested to generate temperature profiles, and an appropriate heating voltage is selected for effective de-icing via distinct avenues of heating system configurations. The heat transfer efficiency of the system is theoretically analyzed and validated through experimental results. The advantages of the carbon-fiber based de-icing system are addressed in terms of weight, flexibility, coverage area, safety and easiness of installation.

Table of Contents

THEESIS REVIEW COMMITTEE	II
ACKNOWLEDGEMENTS.....	III
ABSTRACT	IV
LIST OF TABLES	VIII
LIST OF FIGURES	IX

Chapter I: Introduction

1.1. SIGNIFICANCE OF THE STUDY.....	1
1.2. INTRODUCTION.....	6
1.3. TYPES OF ICE.....	10
1.3.1. CLEAR/GLAZE.....	10
1.3.2. RIME	11
1.3.3. MIXED.....	12
1.4. METHODS OF DE-ICING AND ANTI-ICING SYSTEM.....	12
1.4.1. ANTI-ICING	12
1.4.2. DE-ICING	13
1.4.3. PNEUMATIC DE-ICING BOOTS.....	13
1.4.4. CHEMICAL FLUID.....	14
1.4.5. ELECTRICALLY HEATED SYSTEMS.....	15

Chapter II: Theoretical Background

2.1. NEWTON'S LAW OF COOLING.....	17
2.2. OHM'S LAW.....	19
2.3. JOULE HEATING.....	21

2.4. THERMOCOUPLE	23
2.5. HEAT TRANSFER	25
2.5.1. CONDUCTION	25
2.5.2. CONVECTION	27
2.5.3. RADIATION	27
2.6. COMPOSITES	28

Chapter III: Design Concept

3.1. RESEARCH APPROACH	30
3.2. DESIGN AND PROCEDURES.....	31
3.3. APPARATUS AND MATERIALS	33
3.3.1. HI-CARBON HEATING SOURCE	33
3.3.2. FIBERGLASS	34
3.3.3. THERMOCOUPLE	34
3.3.4. POWER SUPPLY	35
3.3.5. LABVIEW	35

Chapter IV: Theoretical Analysis

4.1. NEWTON'S LAW OF COOLING	37
4.2. OHM'S LAW.....	38
4.3. JOULE HEATING.....	39
4.4. SELF-HEATING EFFECTS.....	41
4.5. THERMAL TIME CONSTANT.....	46
4.6. HEAT TRANSFER	49
4.6.1. THERMAL CONDUCTIVITY	49

4.6.2. HEAT TRANSFER OF THIN PLATE	52
4.7. PREPREG FIBER GLASS CALCULATIONS.....	61

Chapter V: Experimental Analysis

5.1. METHODOLOGY	62
5.2. EXPERIMENTAL DESIGN	65

Chapter VI: Results and Discussion

6.1. APPROXIMATION OF RESISTANCE EQUATIONS	74
6.1.1. BETA (β) PARAMETER	74
6.1.2. STEINHART-HART	76
6.2. EFFECT OF THE NEGATIVE TEMPERATURE COEFFICIENT.....	79
6.3. APPROXIMATION OF HEAT CAPACITY OF THE CARBON FABRIC SYSTEM.....	81
6.4. CARBON FABRIC HEAT GENERATION.....	82
6.5. COMPOSITE LAYER WISE TEMPERATURE	84
6.6. THERMAL CONDUCTIVITY.....	87

Chapter VII: Conclusion and Future Work

7.1. CONCLUSION.....	90
7.2. FUTURE WORK	92
REFERENCES	93
APPENDIX A: 5 LAYERS OF CARBON FABRIC WITH 30 VDC	98
APPENDIX B: 5 LAYERS OF CARBON FABRIC WITH 40 VDC	99
APPENDIX C: 10 LAYERS OF CARBON FABRIC WITH 40 VDC	100

List of Tables

Table 1. In the last decade icing accident	3
Table 2. The linearly independent solutions (Ozisik, 1968).....	57
Table 3. Beta Parameter's approximated resistance values.....	75
Table 4. Steinhart-Hart's approximated resistance values	77

List of Figures

Figure 1. Airplane icing accidents 1987 - 2009 (Duchon, 2010).....	2
Figure 2. Ice on wing leading edge effect (Dillingham, 2010).....	2
Figure 3. Ice formation on aircraft wing structure (Steuernagle, Roy, & Wright, 2002) ...	8
Figure 4. Icicles hang from wing trailing edge in cold environment (Grantz, 2012)	9
Figure 5. Side view of wing with clear ice (Weather)	11
Figure 6. Side view of wing with rime ice (Weather).....	11
Figure 7. Side view of wings with mixed ice (Weather)	12
Figure 8. B.F. Goodrich Pneumatic De-Icing Boots (Flight Safety)	13
Figure 9. Chemical bonding equation of natural rubber	14
Figure 10. Chemical bonding equation of Neoprene	14
Figure 11. Weeping wing: glycol-based chemical fluid seeps through a mesh screen (TKS, 2012)	15
Figure 12. Pitot tube electrical heat diagram (Hudson, 1992)	16
Figure 13. Newton's cooling curve (Forced & Natural Convection).....	18
Figure 14. K-Type thermocouple.....	24
Figure 15. (A) Equilibrium state, (B) One side of heated atoms vibrate, (C) Entire network of atoms vibrate (University, 2002).....	26
Figure 16. Heated particle collide with cold particle.....	26
Figure 17. Description of conduction, convection and radiation (Prucnal, 2013).....	28
Figure 18. Hi-Carbon Prototype 1 on left has five layers of carbon fabric and Prototype 2 on right has ten layers of carbon fabric.....	32

Figure 19. Mesh structure of carbon fabric.....	33
Figure 20. LabVIEW code for the experiment	35
Figure 21. Thermal constant time	48
Figure 22. Schematic sketch of composites direction (Abbey, 2014)	49
Figure 23 Composite region consisting of m layers	54
Figure 24. Carbon black present in Hi-Carbon (Wikipedia, 2015).....	63
Figure 25. Delaminated Hi-Carbon material	64
Figure 26. Laminated Hi-Carbon with glass fiber layers with copper conductive plates. 65	
Figure 27. Vacuum compressed proto types in 260 degree oven	66
Figure 28. Experimental set-up.....	67
Figure 29. Vacuum bag used to hold the carbon fabric, fiberglass layers and thermocouples together	68
Figure 30. Voltage amplifier for generated voltage from thermocouples	69
Figure 31. NI SCB-100 data acquisition (NI Corp.).....	70
Figure 32. Prototypes set-up inside of refrigerator, A specimen is 10 layers of the carbon fabric, and B and C is 5 layers of the carbon fabric.....	70
Figure 33. Burning the specimen A due to the high temperature	71
Figure 34. B and C specimens in the vacuum bag.....	72
Figure 35. Single 5-layer carbon fabric specimen in the vacuum bag.....	72
Figure 36. Comparison of resistance values between Beta Parameter and experimental. 76	
Figure 37. Comparison of resistance values between Steinhart-Hart and experimental .. 78	
Figure 38. Comparison between both approximation method and experimental	78
Figure 39. Experimental currents change over time	79

Figure 40. Theoretical temperature profile of carbon fabric.....	80
Figure 41. Effect of the temperature profile by heat capacity	81
Figure 42. Comparison between experiment and theoretical carbon fabric heat generation temperature profile.....	82
Figure 43. Resistances change over the time.....	83
Figure 44. Temperature profiles of each layer.....	85
Figure 45 One Layer of the Surface Skin Structure.....	86
Figure 46. Comparison Temperature of layer.....	87
Figure 47. Comparison of the temperature with different material	89
Figure 48. Temperature profile for 30 VDC.....	98
Figure 49. Current profile for 30 VDC	98
Figure 50. Temperature profile for 40 VDC.....	99
Figure 51. Current profile for 40 VDC	99
Figure 52. 10 Layers of carbon fabric temperature profile for 40 VDC, around 800s, carbon fabric burned fiberglass.....	100
Figure 53. 10 Layers of carbon fabric current profile for 40 VDC, around the 900s turned power off.....	100

Chapter I: Introduction

1.1. Significance of the study

Aircraft is an invaluable means of transportation for so many aspects of life. In terms of business and travel, aircraft makes it possible to quickly transport large numbers of people and cargo over long distances. Aircraft also have important military applications, with many countries vying for air superiority. Compare the number of fatalities between the war and a transportation aircraft accident. During the Gulf war, 378 UN soldiers were killed in action, but if an Airbus 380 was in an accident, it would kill about 500 passengers in the airplane. Among the safety issues, icing formation can be one of the most dangerous circumstances that could cause catastrophic due to weather.

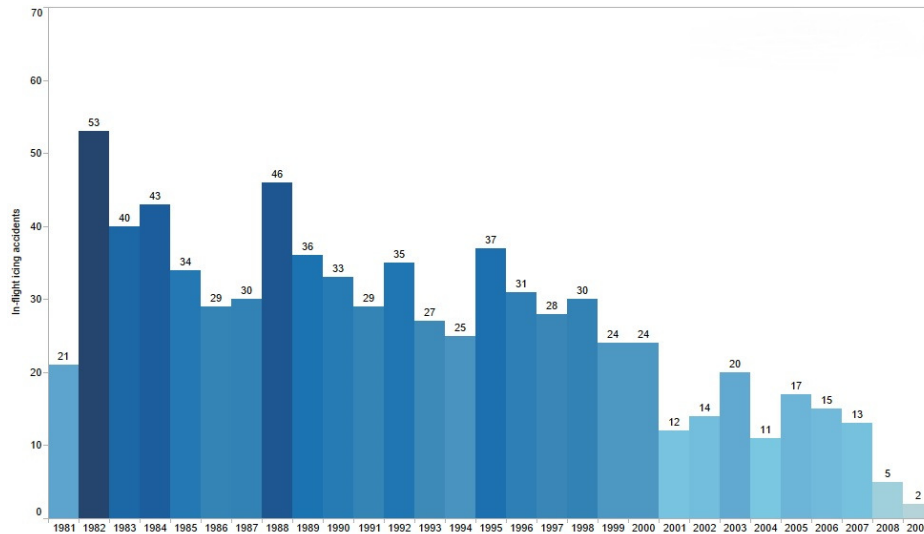


Figure 1. Airplane icing accidents 1987 - 2009 (Duchon, 2010)

As shown in Figure 1, there have been over 750 accidents due to icing from 1981 to 2009. In the last decade, icing accidents have decreased because people have studied the accidents and improved aircraft safety in different weather conditions. Icing can occur over the entire aircraft surface, and this causes a significant negative effect on aerodynamic performance. Most ice formation occurs at stagnation points, such as the nose cone of the aircraft and the wing leading edge. Ice can also form at the turbine engine inlet and on the propeller as well. When there is ice on the wing leading edge, it disrupts smooth airflows and reduces the lift force.

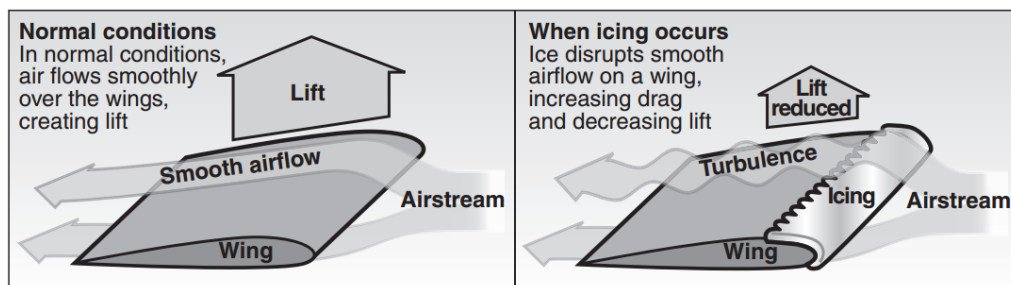


Figure 2. Ice on wing leading edge effect (Dillingham, 2010)

Recently, the new Boeing aircraft B-787 Dreamliner lost thrust while flying due to ice chunks which were sucked into the engine's core. The engines lost power for around five seconds each time any ice chunks were sucked into them. No great harm was caused when this occurred, but the possibility of a serious accident was very high (Freed, 2013).

Occurrences of ice-related accidents are as follows:

1. On April 2nd , 2012, UTAir ATR-72-201 (UTair Flight 120) crashed shortly after takeoff from Tyumen Airport. The accident killed 33 of the 43 people on board. The plane had been parked in freezing weather conditions for eight hours pre-flight and departure without being de-icing (Committee, 2013).
2. On May 18th, 2011, A SOL Linease Aereas Saab 340A was destroyed during the cruise phase. Due to serious aircraft icing, it entered into a stall mode and flew out of control. A total of 19 passengers and three crew members were killed (Hradecky, 2011).
3. On June 1st, 2009, an Air France Airbus A330-203 (AF 447) crashed into the sea after ice crystals blocked the pitot tube during cruising altitude. This accident killed 216 passengers and 12 crew members (BEA, 2012).

Icing-related accidents that have occurred within the last decade are shown below in Table 1. This table contains only accidents that included fatalities.

Table 1. In the last decade icing accident

Date	Type	Registration	Operator	Fatality	Location	Causes
March 04, 2013	Hawker Beechcraft 390 Premier IA	VP-CAZ	Global Jet Luxembourg	2	SE of Annemasse Airport in France	Failure to ground de-icing procedure
April 02, 2012	ATR-72-201	VP-BYZ	UTAir	33	SW of Tyumen Airport in	Failure to ground de-icing

					Russia	procedure
May 18, 2011	Saab 340A	LV-CEJ	SOL Lineas Aereas	22	N of Prahuanien in Argentina	Stall with loss of control due to icing on aircraft
February 04, 2011	Raytheon Hawker 850XP	OD-SKY	Sky Lounge Services	7	Sulaymaniyah International Airport in Iraq	Failure to ground de-icing procedure
November 04, 2010	ATR-72-212	CU-T1549	Aerocaribbean	68	Near Guasimal in Cuba	Pilot failed to manage the icing situation
January 25, 2007	Fokker 100	F-GMPG	Regional Compagnie Aerienne Europeenne	1	Pau-Uzein Airport in France	Loss of control due to ice contamination on the wing surface
June 03, 2006	Shaanxi KJ-200 (Y-8)	Unknown	People's Liberation Army Air Force	40	Near Yaocun in China	Loss of control due to ice contamination on the wing surface
November 19, 2005	Cessna 208B Grand Caravan	P4-OIN	Ivolga-Avia	8	Stupino in Russia	Ice contamination on stall warning system
October 06, 2005	Cessna 208B Super Cargomaster	C-FEXS	Morningstar Air Express	1	SE of Winnipeg Airport in Canada	Over weight flying in icing conditions
February 16, 2005	Cessna 560 Citation V	N500AT	Circuit City Stores	8	Pueblo memorial Airport in USA	Pilot error in managing the icing situation
December 06, 2004	Cessna 208B Grand Caravan	N25SA	Salmon Air	2	S of Bellevue in USA	Pilot error to manage the icing situation
November 28, 2004	Canadair CL-600-2A12 Challenger 601	N873G	Hop-A-Jet Inc	3	Montrose County Airport in USA	Loss of control due to ice contamination on the wing surface
November 21, 2004	Canadair CL-600-2B19 Regional Jet CRJ-200LR	B-3072	China Yunnan Airlines	55	Baotou Airport in China	Failure to ground de-icing procedure
January 17, 2004	Cessna 208B Grand Caravan	C-FAGA	Georgian Express	10	NW of Pelee Island in Canada	Over weight flying in icing conditions
October 29, 2003	Cessna 208B Super Cargomaster	N791FE	Corporate Air	1	Cody-Yellowstone Regional Airport in	Pilot error in managing the icing situation

					USA	
October 03, 2003	Convair CV-580F	ZK-KFU	Air Freight NZ	2	N of Paraparaumu in New Zealand	Beyond the capability of the anti-icing system
April 08, 2003	Dassault Falcon 20	N183GA	Grand Aire Express	3	W of Toledo in USA	Failure to turn on the anti-icing system
December 21, 2002	ATR-72-202	B-22708	Trans Asia Airways	2	SW of Makung City in Taiwan	Pilot error in managing the icing situation
November 08, 2002	Cessna 208B Grand Caravan	N514DB	Brown County Financial Services	4	S of Parks in USA	Pilot error in managing the icing situation
March 15, 2002	Cessna 208B Super Cargomaster	N228PA	Priority Air Charter	1	S of Alma in USA	Failure to ground de-icing procedure
January 04, 2002	Canadair CL-600-2B16 Challenger 604	N90AG	Epps Air Service	5	Birmingham International Airport in United Kingdom	Failure to ground de-icing procedure
December 26, 2001	Pilatus Britten-Norman BN-2B-26 Islander	D-IAAI	BAL Bremerhaven Airline	8	Bremerhaven Airport in Germany	Failure to ground de-icing procedure
October 10, 2001	Cessna 208 Caravan I	N9530F	Penair-Peninsula Airways	10	Dillingham Municipal Airport in USA	Loss of control due to ice contamination on the wing surface
May 05, 2001	Cessna 208B Super Cargomaster	N948FE	Corporate Air	1	S of Steamboat Springs Airport in USA	Pilot error in managing the icing situation
April 28, 2001	Cessna 208B Grand Caravan	LV-WSC	Les Grands Jorasses	10	Roque Perez in Argentina	Pilot error in managing the icing situation with overweight flying in icing conditions
March 09, 2000	Yakovlev 40D	RA-88170	Vologoda Air	9	Moskva-Sheremetyevo Airport in Russia	Pilot error in managing the icing situation with failure to ground de-icing situation
January 13, 2000	Shorts 360-300	HB-AAM	Sirte Oil Company	22	Marsa el-Brega in Libya	Failure to turn on the anti-icing system

As shown in Table 1, aircraft accidents due to icing have killed 338 passengers and crew members in the 2000s. According to the Table 1, more than two-thirds of the accidents occur by failure to de-icing procedure of the aircraft before flight.

1.2. Introduction

Over the last decade, carbon has been used in many different applications, including its use in electric heating elements. Most of the limited literature that is available provides information about electrical properties of carbon fibers, and a few numbers of literatures discuss about the carbon but not a carbon fiber such as carbon cloth and carbon fabric. There is also literature about the modification or integration of fibers to make intelligent fabric. In the 1970's, activated carbon cloth was developed and originally used in military clothing for protection against biological and chemical agents. Activated carbon cloth can also be used as a high quality filter to trap the organic or inorganic molecules of harmful gases and liquids. It is a good ohmic conductive material as well.

Subrenat and Cloirec conducted experiments to study the electrical thermal behavior of activated carbon cloths by the Joule effect (Subrenat & Cloirec, 2003). They found that the temperature distribution of activated carbon cloth is very homogeneous at the surface. It has low resistance values due to the high carbon contents of carbon (Kim & Chung, 2003). In their experiment, they used carbon fiber mats, composed of discontinuous carbon fibers that were randomly oriented in two dimensions, as it is less expensive than the continuous carbon fiber.

Fosbury et al. conducted further studies on carbon fiber as a heat resistant element (Fosbury, Wang, Pin, & Chung, 2003). They used the interlaminar interface of a carbon fiber polymer-matrix composite. Their system consumed power and was very effective at resistance heating. By using the interlaminar interface shape, they improved the heat resistance system by reducing the mass of the volume.

Falzon et al. studied about the anti-icing and de-icing techniques by using a carbon-based electro conductive textile as a heat source and fiberglass to possibly preventing electrical shorting (Falzon, Robinson, Frenz, & Gilbert, 2015). But the problem of this system was electrical shorting still occurred when the panels were exposed to external impact energies.

Bhat et al. also studied the use of intelligent fabrics as electrically conductive material, but they used something other than carbon (Bhat, Seshadri, Nate, & Gore, 2006). They employed a method of diffusion of pyrrole for impregnating polypyrrole into cotton fabrics to be used as electrical heating elements. Due to the flexibility of their system, they were able to use the cotton fabrics to create heating pads and integrate it into material used to make apparel. Their system and the proposed carbon fabric de-icing system have some similarity in that they used the polypyrrole to make conductive material instead of using the carbon powder. The problem of this system is the low temperature increment, which means the temperature increases very slowly.

Research was conducted on carbon fiber heating patents on file with the U.S. Patent office about carbon powder. Most of the patents pertained to the thermal conductivity of carbon powder, but not combination of carbon powder and cotton mesh screen to make a heating element.

There are different De-icing system techniques available, yet they all serve to avoid the accumulation of ice on aircraft surfaces. The formation of ice on the wing structure of an aircraft is a major hazard and danger in aviation. For instance, as shown in Figure 3, the formation of ice on the wing leading edge generates a highly non-laminar fluid flow over the wing structure, which in turn produces drag, a loss of lift, and control and possible stalling of an aircraft during in-flight conditions.

Several reported incidents over the past few years have been caused by icing on a wing part of an aircraft. For example, on November 17, 1988, the B-1b bomber crashed at Ellsworth Air Force Base by an uncontrollable wing due to ice formation on its wings (Evans, 1988). Scientists and engineers have acknowledged that ice primarily forms on an aircraft flying when temperatures are below 32°F, and aerodynamic cooling may generate icing at a few degrees higher than this. These ice formations on the aircraft wing leading edges are classified into three different types: clear hard and glossy, rime-brittle and frost-like, and mixed-hard and rough conglomerate ice. The detail images of the three different ice formations are shown in Figure 5, Figure 6, and Figure 7.



Figure 3. Ice formation on aircraft wing structure (Steuernagle, Roy, & Wright, 2002)

The first type of ice formation is the clear-hard and glossy ice, which is occasionally transparent form. This type of ice exhibits a porous quality from air pockets within which are very dense and complex to remove. The second type of ice formation is the rime-brittle with frost-like ice, which has a brittle quality with a rough surface and is consequently easier to remove than clear ice. The third type of ice formation is the mixed ice, and it consists of both clear and rime mixed. Therefore, it consists all of all the ice properties as a result (Conrad, 2010).



Figure 4. Icicles hang from wing trailing edge in cold environment (Grantz, 2012)

Currently, different de-icing systems are extensively employed on aircraft components using various techniques. Among such are resistance heated, air heated, weeping wing, boot and electrically heated de-icing; which all entail unique heating efficiency, aircraft-type compatibility and due cost. Note the primary objective of these de-icing systems is to remove and prevent the ice on the wing leading edge and control surface as shown in Figure 4.

Electrically heated systems are familiar commodities outside of the aerospace industry which may rely on graphite-based materials that quickly heat and cool down

easily. The prime advantage of this system is that they are very lightweight de-icing materials. These systems are widely popular and utilized in the civil industry due to their performance of energy consumption. For electric heating systems, they are traditionally used either by heating wires or by graphite heaters. Yet, new carbon heating system sheets sustain enhanced performance and a higher safety rating. For instance, the Kelly Aerospace Thermal Systems manufactured a flexible carbon heating film for their THERMAWING systems (Cahalin, 2011), as opposed to electric systems that ceases to function in an open circuit due to a conducting path severance. Carbon heating systems may continue operating after having suffered mid-sheet lacerations since there are several conductive paths of possible current flow. Additionally, carbon heating systems sheets are very flexible and can support protean application. Similar in versatility and conductivity to this sheet is the carbon heating fiber system, which has become a major solution in the new frontier of aircraft de-icing systems.

1.3. Types of Ice

There are mainly three types of ice contaminates that occur on an airplane's surface are; clear/glaze, rime, and mixed.

1.3.1. Clear/Glaze

The first type of ice formation is clear-hard and glossy ice which is occasionally transparent. Clouds sometimes contain large drop sizes of concentrated liquid water. When these water drops do not freeze at temperature below 0°C, they are referred to as supercooled water. This happens when the nucleation process fails. When such large

supercooled water droplets come in contact with the cold surface of an aircraft, they freeze into a clear ice form. This type of ice contains air pockets which give it a porous quality and make it difficult to remove. Clear/glaze is the most dangerous form of icing (Weather).



Figure 5. Side view of wing with clear ice (Weather)

1.3.2. Rime

The second type of ice formation is rime-brittle and frost-like ice. When small supercooled water droplets come in contact with the cold surface of an aircraft at sub-zero temperatures, they form rime ice. This type of ice has a brittle quality with a rough surface and is subsequently easier to remove than clear ice. The formation of rime ice is white and rough frost is forming on an aircraft (Weather).

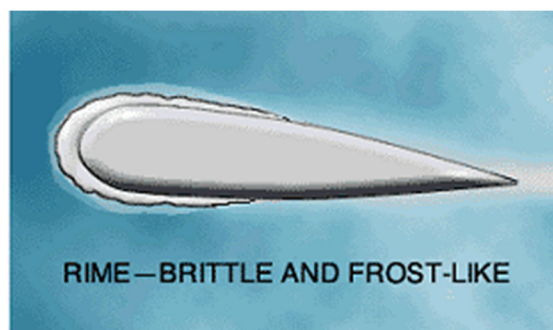


Figure 6. Side view of wing with rime ice (Weather)

1.3.3. Mixed

Lastly, mixed ice consists of both clear and rime mixed together.

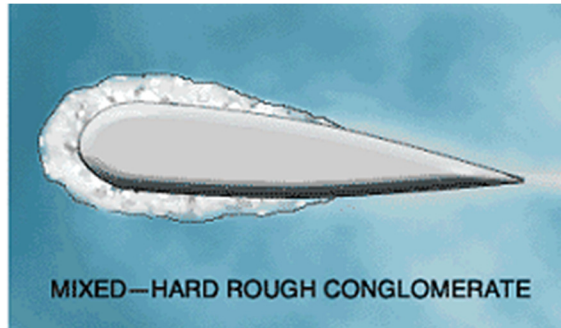


Figure 7. Side view of wings with mixed ice (Weather)

1.4. Methods of De-Icing and Anti-Icing System

De-icing systems are employed on a vast number of aircraft using a variety of methods. Among such methods are air heated, resistance heated, boot, weeping wing and electrically heated de-icers; all of which entail unique heating efficiency, aircraft-type compatibility and due cost. Note the primary objective of these methods is to de-ice only the wing leading edge.

1.4.1. Anti-Icing

The purpose of anti-icing is to prevent the formation of frost or ice on the surface of aircraft for a limited amount of time (Buck, 2004). Examples of anti-icing systems are thermal heat, prop heat, pitot and static ports tube heat, fuel vent heat, windshield heat, and fluid surface de-icers.

1.4.2. De-Icing

De-icing is the removal of frost or ice formations after they begin to form on the surface of an aircraft (Buck, 2004). De-icing includes systems such as de-icing boots, weeping wing, mechanical, and electrical heat.

1.4.3. Pneumatic De-Icing Boots

Pneumatic de-icing boots were invented by B.F. Goodrich Corporation in 1923. A novel de-icing system can be seen in Figure 8. Boots are effective when used with light aircraft, whereby they employ a rubber membrane inflated by compressed air to break ice formations on wing surfaces. De-icing boots, nevertheless, must be replaced every two to three years and are subject to membrane puncture that renders the boot ineffective.

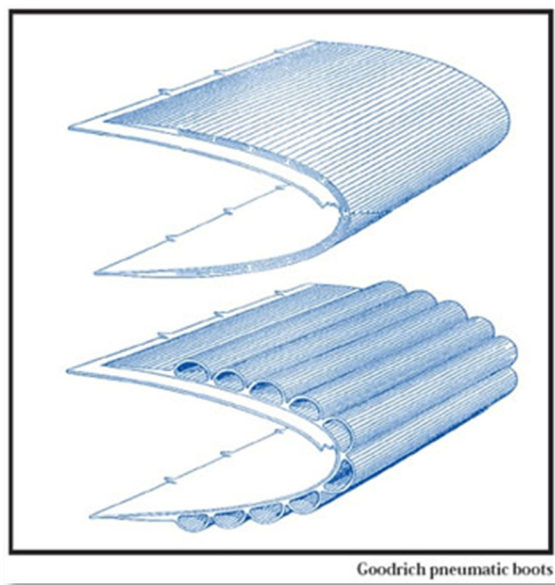


Figure 8. B.F. Goodrich Pneumatic De-Icing Boots (Flight Safety)

All of the pneumatic de-icing boots systems from B.F. Goodrich Corporation possess reliable features that give superior performance. The boots are made of black

neoprene, a material invented by DuPont scientists in 1930 (Shenai-Khatkhate, 2013). Neoprene provides better protection from ozone, oxidation and erosion than natural rubber because of its molecular formation. The chains of double bonds are in much smaller proportion compared to rubber, as Figure 9 and Figure 10 (Tobias & Koenigsberger, 1970).

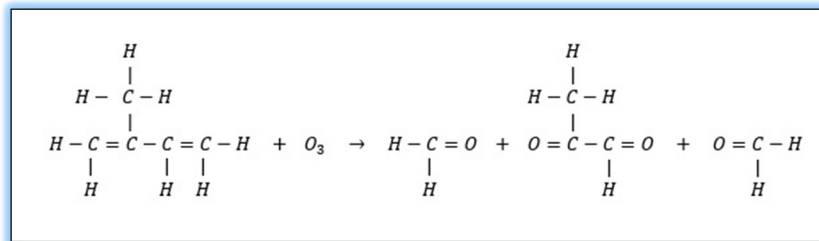


Figure 9. Chemical bonding equation of natural rubber

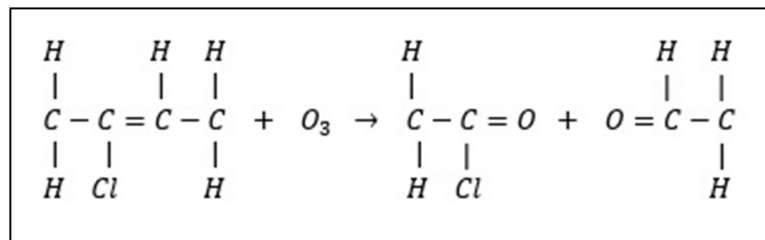


Figure 10. Chemical bonding equation of Neoprene

1.4.4. Chemical Fluid

Weeping wing systems protect wings from ice formation through a glycol-based chemical fluid that seeps through a mesh screen and coats the wing surface. The glycol-coated wings prove to be effective in both removing and preventing ice formations.



Figure 11. Weeping wing: glycol-based chemical fluid seeps through a mesh screen (TKS, 2012)

1.4.5. Electrically Heated Systems

Electrically heated systems consist of graphite-based materials that may quickly be heated and cooled with at ease. The primary advantage of these systems is that they are lightweight de-icers. These systems are also popular in the civil industry due to their high performance and low energy consumption. Electric heating systems traditionally use either heating wires or graphite heaters; however, new Hi-Carbon heated sheets sustain improved performance and a higher safety rating. The Kelly Aerospace Thermal Systems developed a flexible carbon heating film for their ‘Thermawing’ system.

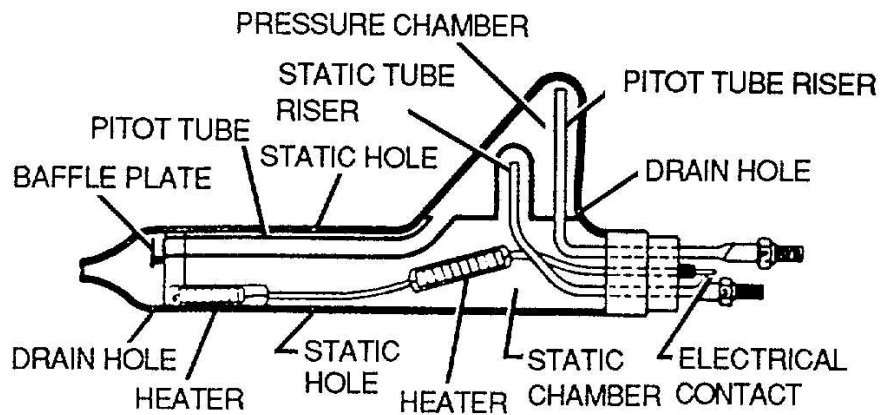


Figure 12. Pitot tube electrical heat diagram (Hudson, 1992)

Most modern electrically heated systems are using the resistance heating wire that made by nichrome. Other than the aerospace field, this wires are broadly using for the heater because it has great energy efficiency and small amount of weight increases are not critically effect, but in the aerospace industry, weight is directly related with range, speed, fuel economy, durability and safety factor. Thus, this wires are usually using for small devices as shown in Figure 12.

Chapter II: Theoretical Background

2.1. Newton's Law of Cooling

In 1701, Sir Isaac Newton developed the formula for the transfer of heat from one place to another. The meaning of Newton's Law of Cooling is "*The rate of cooling of a warm body at any moment is proportional to the temperature difference between the body and its surrounding medium (air)*" (Cheng & Fujii, 2007).

By using a linseed oil thermometer and fusion points of alloys and metals, Newton performed transient heat conduction experiments with turbulent forced-convection cooling. Thus, he obtained the Newton's Cooling Curve, as shown in Figure 13. From the Newton's law of cooling, the rate of the heat energy loss can be obtained.

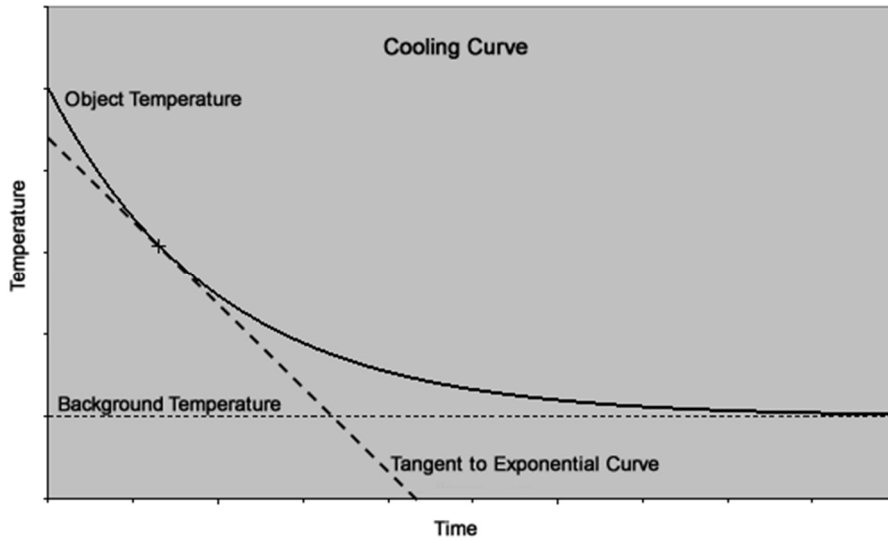


Figure 13. Newton's cooling curve (Forced & Natural Convection)

When the object temperature T is directly proportional to the difference in temperature between the object and background, it can express the following equation with proportionality constant of k in small rate of change.

$$\frac{dT}{dt} = k(M - T)$$

Eq. 2. 1. 1

- T: Object Temperature
- M: Background Temperature
- k: Proportionality Constant

By differential equations by separating variables, Eq. 2. 1. 1 can be rewritten as below,

$$\frac{dT}{M - T} = kdt$$

Eq. 2. 1. 2

Integrating both sides,

$$\int \frac{1}{M - T} dT = \int kdt$$

Eq. 2. 1. 3

$$-\ln|M - T| = kt + C$$

$$\ln|M - T| = -kt - C$$

$$|M - T| = e^{-kt-C} \quad \text{Eq. 2. 1. 4}$$

When the object temperature is higher than the background temperature ($T > M$), $M - T$ is negative, so Eq. 2. 1. 4 can be expressed as follows,

$$-(M - T) = e^{-kt-C} \quad \text{Eq. 2. 1. 5}$$

$$T = M + e^{-kt-C}$$

$$T = M + Ae^{-kt}, \quad \text{where } A = e^{-C} \quad \text{Eq. 2. 1. 6}$$

When the object temperature is lower than the background temperature ($M > T$), $M - T$ is positive, so Eq. 2. 1. 4 can be expressed as follows,

$$(M - T) = e^{-kt-C} \quad \text{Eq. 2. 1. 7}$$

$$T = M - Ae^{-kt}, \quad \text{where } A = e^{-C} \quad \text{Eq. 2. 1. 8}$$

In Eq. 2. 1. 6, above, the object is cooling down to the background temperature, and in Eq. 2. 1. 8, the object is warming up to the background temperature.

2.2. OHM's Law

In 1827, George Ohm published the book *Die galvanische Kette, mathematisch bearbeitet* (The Galvanic Circuit Investigated Mathematically), in which he stated “*the currents furnished by different galvanic cells, or combinations of cells, are always directly proportional to the e.m.f.'s existing in the circuits in which the currents flow, and*

inversely proportional to the total resistances of these circuits” (Millikan & Bishop, 1917). The complete circuit can describe by OHM’s law as shown in below equation:

$$I = \frac{E}{R} \quad \text{Eq. 2. 2. 1}$$

- I: Current in amperes (*A*)
- E: ElectroMotive Force (e.m.f.) in volts (*V*)
- R: Resistance of the circuit in ohms (Ω)

As shown in the Eq. 2. 1. 1, the equation can be written as any portion of an electrical circuit as in the equation below:

$$I = \frac{P.D.}{r} \quad \text{Eq. 2. 2. 2}$$

- P.D.: Potential difference between any two points in volts
- r: Resistance of the conductor connecting these two points in ohm

Both of the equations above can be represented as one equation as which is listed below.

This is most important law in physics (Millikan & Bishop, 1917).

$$\text{Amperes} = \frac{\text{Volts}}{\text{Ohms}} \quad \text{Eq. 2. 2. 3}$$

Ohm’s law can be expressed as three varying equations:

$$I = \frac{V}{R} \quad \text{Eq. 2. 2. 4}$$

$$\text{or } V = I \cdot R \quad \text{Eq. 2. 2. 5}$$

$$\text{or } R = \frac{V}{I} \quad \text{Eq. 2. 2. 6}$$

2.3. Joule Heating

Joule heating is referred to as Ohmic heating, electrical resistance heating or electro conductive heating. James Joule found that heat from mechanical work relates to Ohm's Law. And when Lord Kelvin (William Thomson) developed the absolute temperature scale (Kelvin, K), he decided to collaborate with Joule. Together, they developed a thermodynamic effect called the Joule-Thomson effect, or the Joule-Kelvin effect. In order to express heat energy in the same unit as mechanical and electrical energy, the Joule became the standard unit of measurement. A Joule is the amount of work done raise the temperature of water 1°F required same amount energy all the time, and thermal energy is generated via per unit time (\dot{E}):

$$\dot{E} = I^2 \cdot R \quad \text{Eq. 2. 3. 1}$$

- \dot{E} : Thermal energy per unit time ($\frac{J}{s}$)

The thermal energy is proportional to the square of the current and the resistance. And in electrical power, thermal energy per unit time is the instantaneous power (P) in watts (W). Using Eq. 2. 3. 1 and Eq. 2. 2. 4, three different equations can be derived,

$$P = I^2 \cdot R \quad \text{Eq. 2. 3. 2}$$

$$\text{or } P = \frac{V^2}{R} \quad \text{Eq. 2. 3. 3}$$

$$\text{or } P = V \cdot I \quad \text{Eq. 2. 3. 4}$$

Theoretically, when power is constant the delivered energy (E) in time (t) can be described as:

$$E = P \cdot t \quad \text{Eq. 2. 3. 5}$$

$$E = V \cdot I \cdot t \quad \text{Eq. 2. 3. 6}$$

When electrical energy is applied to a resistor, the electrical energy changes into the form of heat (Q) in calorie (cal). The amount of heat energy produced can be measured by using a calorimeter. The joule is the energy required to change one gram (g) of a substance's temperature (ΔT) by one degree Celsius ($^{\circ}\text{C}$).

$$Q = m \cdot c \cdot \Delta T \quad \text{Eq. 2. 3. 7}$$

- Q : Heat in calories (cal)
- m : Mass of a substance in kilograms (Kg)
- c : Specific heat capacity in joules per Celsius kilogram $\left(\frac{J}{^{\circ}\text{C}\cdot\text{Kg}}\right)$
- ΔT : Change in temperature in Celsius ($^{\circ}\text{C}$)

With Eq. 2. 3. 7, the heat (Q) can be converted to the joule by using the conversion factor of joules to calories (J) as shown below;

$$E = J \cdot Q \quad \text{Eq. 2. 3. 8}$$

- J : Conversion factor of joules to calories in joule per calorie $\left(\frac{J}{\text{cal}}\right)$

Using Eq. 2. 3. 6 and Eq. 2. 3. 8, two energy equations can be expressed as

$$V \cdot I \cdot t = J \cdot Q$$

$$\therefore Q = \frac{V \cdot I \cdot t}{J} \quad \text{Eq. 2. 3. 9}$$

2.4. Thermocouple

In 1821, the German-Estonian physicist Thomas Johann Seebeck determined the principle of the thermoelectric effect, also called the Seebeck effect. This effect can be observed by the voltage that is generated when a metal is subjected to a thermal gradient.

A thermocouple is one of the most widely used temperature sensors and is made by connecting two dissimilar conductors together at one end. The point where the two dissimilar metals join is called the measurement junction or hot junction. At the other end, the unjoined wires are connected to the signal conditioning circuitry traces, which are typically made of copper. The area between the thermocouple metals and the copper wire is called the reference junction or cold junction. Whenever there is a temperature change at a hot junction a voltage is generated in the metal. This principle of thermocouples is called thermal electromotive force (EMF), which is expressed as the following equation:

$$e = \alpha(T_{sense} - T_{ref}) \quad \text{Eq. 2. 4. 1}$$

- e : Thermo electromotive force
- α : Seebeck coefficient

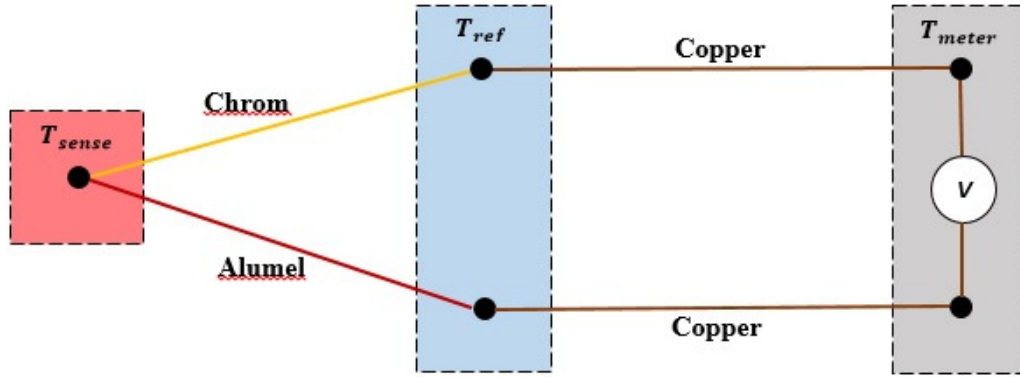


Figure 14. K-Type thermocouple

The K-type thermocouple temperature sensor consists of a combination of Chromel (90% nickel and 10% chromium) and Alumel (95% nickel, 2% manganese, 2% aluminum and 1% silicon). The K-type thermocouple generates approximately $41\mu V/K$. As shown in Figure 14, the voltage output V_{out} can be derived from the equation shown below:

$$\begin{aligned}
 V_{out} &= \int_{meter}^{ref} S_{copper}(T) \frac{dT}{dx} dx + \int_{ref}^{sense} S_{chromel}(T) \frac{dT}{dx} dx \\
 &+ \int_{sense}^{ref} S_{alumel}(T) \frac{dT}{dx} dx + \int_{ref}^{meter} S_{copper}(T) \frac{dT}{dx} dx \\
 &= \int_{T_{ref}}^{T_{sense}} S_{chromel}(T) dT + \int_{T_{sense}}^{T_{ref}} S_{alumel}(T) dT \\
 V_{out} &= \int_{T_{ref}}^{T_{sense}} [S_{chromel}(T) - S_{alumel}(T)] dT
 \end{aligned}$$

Eq. 2. 4. 2

- $S_{chromel}$: Seebeck coefficient of the chromel
- S_{alumel} : Seebeck coefficient of the alumel

$S(T)$ is the temperature-dependant Seebeck coefficient of each conductor. By using the output voltage and reference temperature, thermocouple can determine temperature that where interest.

2.5. Heat Transfer

There are three types of heat transfer as conduction, convection and radiation. Heat transfer is thermal energy that flows from a hot area to a cold area. It is similar to pressure in that air flows from an area of high pressure to an area of low pressure until the pressure becomes balanced in both areas. When there are two different bodies with different temperatures, thermal energy is transferred by flowing the body of higher temperature body to lower temperature.

2.5.1. Conduction

When heat is transferred through solid or stationery fluids, it is called conduction heat transfer. There are two mechanisms that explain conduction heat transfer. The first is, Lattice vibration, which is a vibrating superimposed network of atoms. When force is applied to an atom, the atom them moves other atoms to return to the equilibrium position, and during that motion, the entire network atoms vibrates (Tsymbol, 2005).

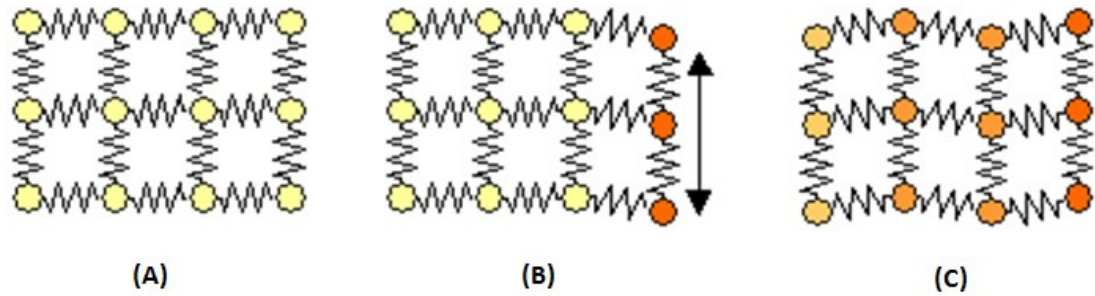


Figure 15. (A) Equilibrium state, (B) One side of heated atoms vibrate, (C) Entire network of atoms vibrate (University, 2002)

In the Figure 15 (A) shows the equilibrium state which means there are no temperature difference in the interest body. When thermal force applied, atoms start vibrating as shown in Figure 15 (B), and these vibrations vibrate entire network of atoms. This mechanism shows the transferring the thermal energy as shown in Figure 15 (C).

The second mechanism that explains conduction heat transfer is particle collision. Heated particles are move around inside of a body, and collide with cold particles, which transfer the heat energy.

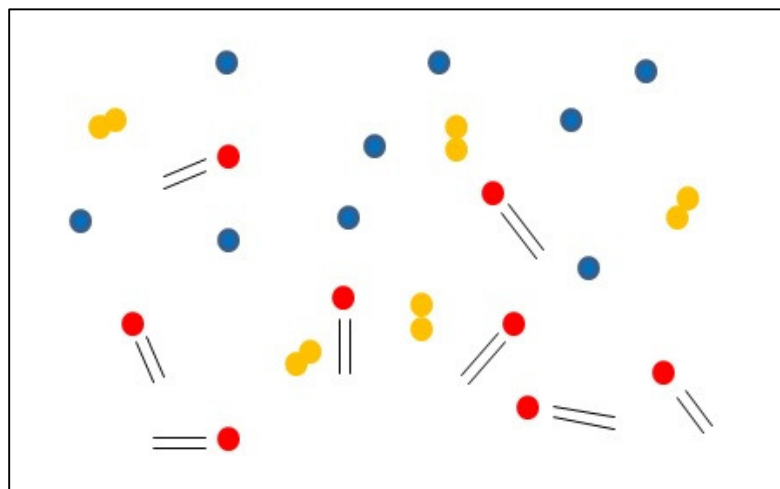


Figure 16. Heated particle collide with cold particle

The general equation for conduction heat transfer equation is;

$$q = -k \cdot A \cdot \frac{\Delta T}{\Delta x} \quad \text{Eq. 2. 5. 1}$$

where k is the thermal conductivity, A is cross-sectional area (Holman, 2010).

2.5.2. Convection

Convection heat transfer is the thermal energy transferred between the solid and surrounding air or liquid. Another name for convection is Newton's law of cooling as described at in section 2.1.

2.5.3. Radiation

Radiation does not require an intervening medium to propagate. It transfers heat by electromagnetic waves (or photons) thus it can transfer heat in a vacuum. This is the only form of heat transfer that can occur in a vacuum. The general equation for radiation heat transfer is;

$$q = \varepsilon \cdot \sigma \cdot A \cdot T_b^4 \quad \text{Eq. 2. 5. 2}$$

where ε is the emissivity ($0 \leq \varepsilon \leq 1$), σ is the Stefan-Boltzmann constant, and T_b is the temperature of the body.

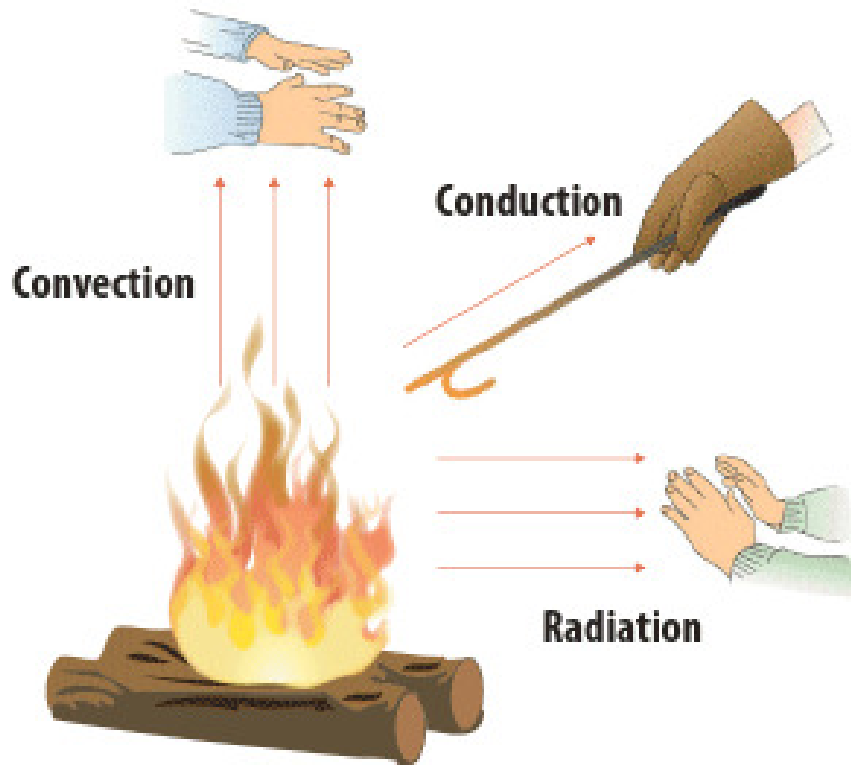


Figure 17. Description of conduction, convection and radiation (Prucnal, 2013)

Through the campfire image shown in Figure 17, we can understand the general meaning of conduction, convection and radiation. Conduction is heat that transfers through solid material, convection is heat that flows in the surrounding air or liquid, and radiation is heat that can be emitted anywhere.

2.6. Composites

Two or more different materials are combined on a macro scale to form a single structure material, and change the properties of the materials called a composite material. Also we treat composite as homogenous but not an isotropic material. The major types of

composite materials are fibrous, laminated, particulate, or combination of some or all of them.

In the 1500s B.C., early Egyptians and Mesopotamian settlers were the first to use composite material. They mixed mud and straw to build strong and durable buildings, pottery, and boats. Later, in 1200 A.D., Mongolians used wood, bone and animal glue to invent the first composite bow. In the early 1900s, plastics were developed, which brought about a huge change. Plastic itself does not have great strength, but when combined with other materials, it becomes a very strong structure, such as a fiber reinforced polymer (Johnson, 2015).

Glass fiber is the most common substance in composite material. There are several types of glass fibers such as A, E, C, D and S-glass. A-glass contains high **Alkali** glass that degrades electrical properties. E-glass has very good **Electrical** insulation properties and is mainly used in textile glass production because of its low alkali content. C-glass has good **Corrosion** resistant qualities, which means it is chemical resistant. S-glass has 33% higher tensile **Strength** than E-glass. And D-glass has the greatest electrical insulation properties with low dielectric constant (Lee, 1989).

Composite materials properties are changing depend on which material combined in the composite. As mentioned about the glass fiber, depending on the purpose of usage, it can easily change the material properties by combining other materials.

Chapter III: Design Concept

3.1. Research Approach

Nowadays, many of the aircraft manufactures are using the composite material because it has great strength to weight ratio. For the thermal protection system wing often employed the reinforced carbon-carbon fiber and for stressed-skin wing designs, honeycomb structure employed with difference materials of core and outer skin such as aluminum, Aramid fiber coated with Phenolic, fiberglass, plastic, Nomex, Kevlar and carbon fiber. For the sake of manufacturing simplicity, thermal and mechanical characteristics, and advantages over aluminum and vinyl, the fiberglass composite was selected for constructing the wing leading edge (Nadel, 2006).

Similarly, the system material was selected on a multi-basis case. As opposed to many other de-icing systems, the Hi-Carbon fabric requires minimal additional equipment, thus reducing aircraft volume and mass load. The de-icing boot technique requires tanks of compressed air and additional piping, while the sweep wing technique requires de-icing chemical agents, all of which incur additional aircraft weight.

Mechanical and chemical de-icing systems sometime leave some ice un-melted, a flaw that does not occur with the properly powered Hi-Carbon fabric. The minimalistic Hi-Carbon de-icing system is thin and lightweight even when compared to other electrical heating devices, deeming it optimal for aircraft de-icing applications.

The Hi-Carbon heating fabric was manufactured with the specification of attaining a temperature of 100°F (38°C) in 60 seconds under an applied 15A, 120VAC power source. The initial prototype designs consisted of, firstly, a Hi-Carbon fabric sandwiched between fiberglass composite layers and, secondly, a fabric attached to the innermost of eight composite layers on the wing leading edge. Since the two conceptual designs differed in the location of the heating system within the composite, the response times were assumed to vary for each; an increasing distance of the fabric to the wing surface yields a slower target temperature attainment. Accordingly, the first design was expected to be desirable for its rapid response time while the second design was expected to be desirable for its ease of application onto existing leading edges. Alternatively, the first design was expected to pose more difficulty in the direct application onto existing leading edges while the second design was expected to produce a slower heat transfer rate onto the wing surface.

3.2. Design and Procedures

In the Materials Testing Laboratory at Embry-Riddle Aeronautical University, two distinct leading edge prototypes were constructed. The composite laminates are made

of prepreg fiberglass for each prototype due to the abundance of available prepreg and lack of epoxy and hardener.

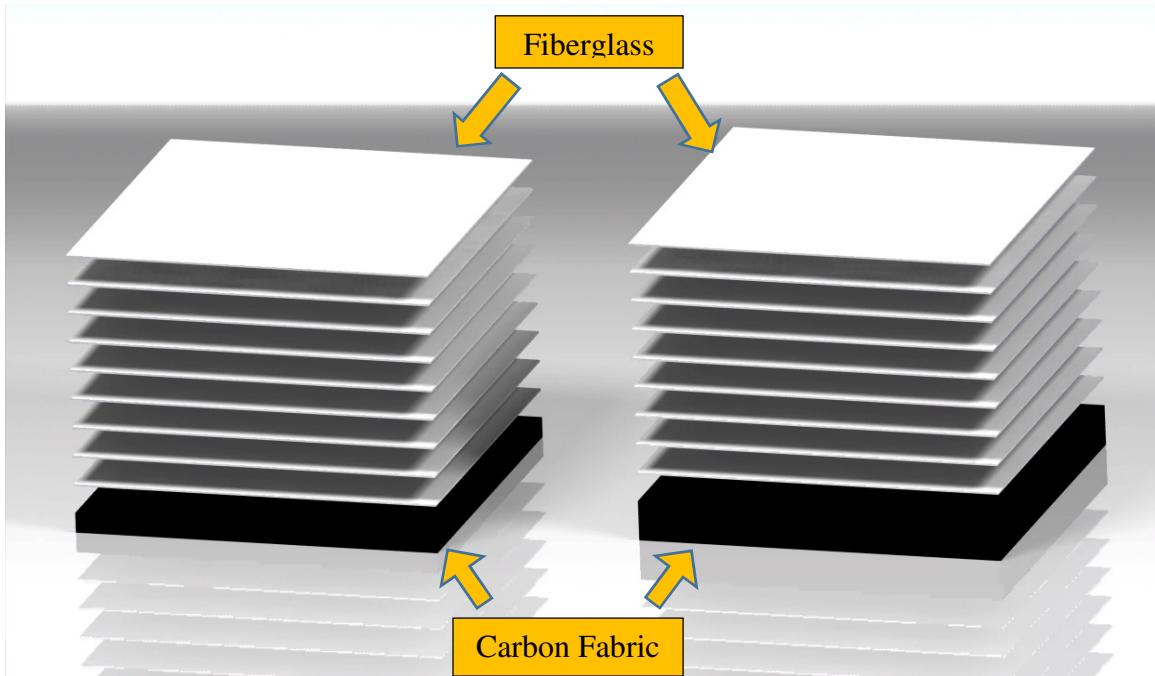


Figure 18. Hi-Carbon Prototype 1 on left has five layers of carbon fabric and Prototype 2 on right has ten layers of carbon fabric

For the first prototype, the heating fabric, folded five times, was in thermal contact with one composite layer towards the bottom side of the plate and ten composite layers on top side of the fabric.

For the second prototype, the heating fabric, folded ten times, was in thermal contact with one composite layer towards the bottom side of the plate and ten composite layers on the top side of the fabric.

3.3. Apparatus and Materials

3.3.1. Hi-Carbon Heating Source

A Hi-Carbon Heating source is a radiant floor heating system composed of a cotton fiber weave impregnated with carbon. It has a low noise level and is a flexible material (HiCARBON, 2011). An advantage to this material is that when it gets damaged or some sections at the heating portion get cut off, it would still work properly due to the mesh structure as shown in Figure 19



Figure 19. Mesh structure of carbon fabric

Compared to other electrical heating sources, Hi-Carbon has high weight to area ratio because Hi-Carbon structures consist mainly of woolen fabric. Also, this product is cheap to produce in large quantities.

3.3.2. Fiberglass

Last decade, many of the aircraft skin structures were designed and made by the conductive aluminum material. The carbon heating system uses the electric power to generate heat. Therefore, carbon fabric cannot be attached to the aluminum structure since it might short out the electrical system.

For attaching those two materials, non-conductive material is required. In order to maintain the flexibility of carbon fabric, the non-conductive material must be flexible too. As mentioned in section 2.6 mentioned about the E-glass (Fiberglass) has great electrical insulation property, also E-glass has great flexibility due to the material property until it cures. Each side of the carbon fabric is therefore covered with E-glass to avoid short circuit.

3.3.3. Thermocouple

For measuring the temperature of the specimen, type-K (chromel-alumel) thermocouple is selected because the K-type of thermocouple is inexpensive and has a wide measuring temperature range. This thermocouple has great operation temperature range for these experiments. Thermocouple is good approximate measuring temperature sensor, because it is difficult to measure the temperature within one degree error. But due to the wide measuring temperature range with cost effect, it is variety using in many area for temperature sensor. But it can increase accuracy by using the voltage amplifier.

3.3.4 Power Supply

In this experiment, a constant voltage of 20 V is used to obtain high performance characteristics from the materials. The higher the voltage makes reaching the higher maximum temperature, and the higher the slope or temperature increment, and hence it allows shorter time to reach the final temperature.

3.3.5. LabVIEW

LabVIEW is one of the mostly used engineering tools in measurement or control of the application. This software uses the box diagram for easier and visualizes constructing the algorithm.

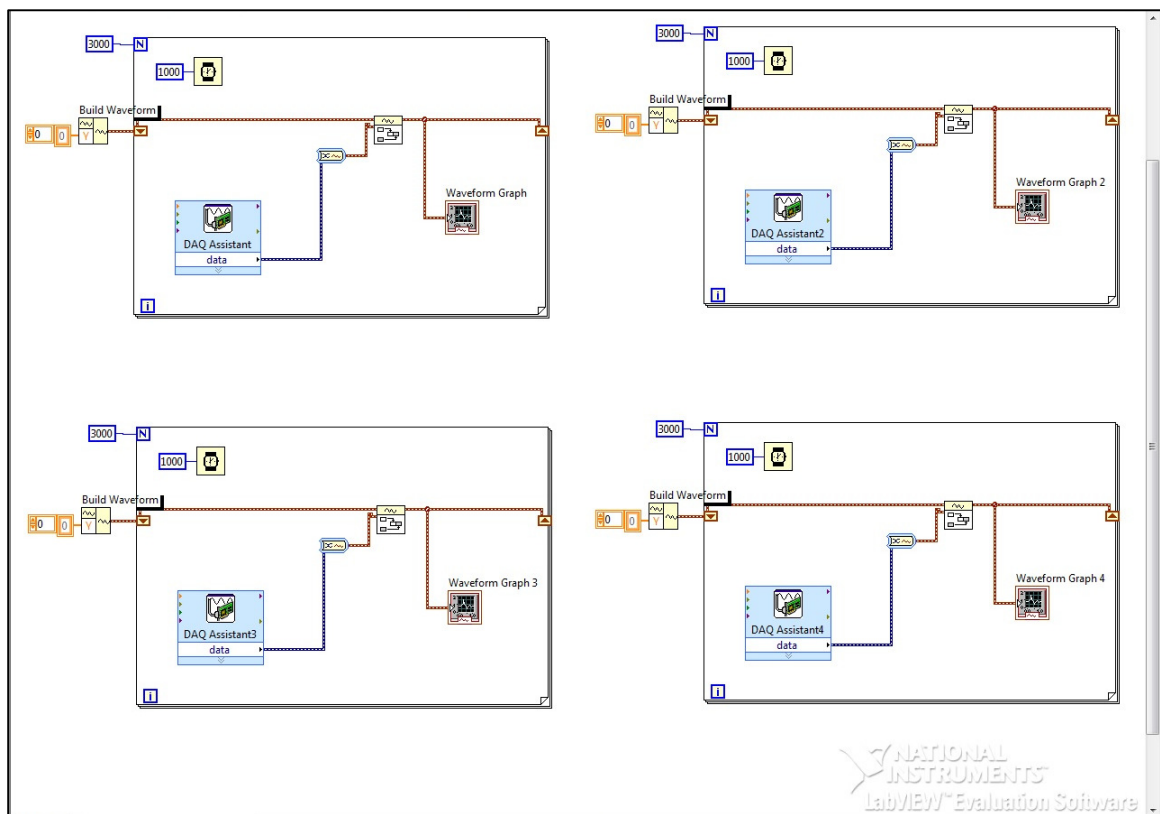


Figure 20. LabVIEW code for the experiment

In this experiment, LabVIEW is used for measuring the temperature by sending and receiving analog voltages and temperature data through a data acquisition system. As shown in Figure 20, four different loops are collecting the data from each sensor every second for 3000 seconds and it is automatically drawing the temperature profile according to the time.

Chapter IV: Theoretical Analysis

4.1. Newton's Law of Cooling

To more intuitively fathom the thermal properties of the Hi-Carbon system, the following sections delve into the theoretical underpinnings of the system in regards to the fluctuation-dissipation theorem.

As the heating system is applied onto the wing composite structure, thermal energy is also applied as heat fluxes, which acts to transverse the structure and de-ice the wing surface. The convective rate of heat generated and lost by the heating system in an infinitesimally small time interval, dt , is proportional to the temperature difference between the heating system and the wing leading edge surface, as given by Newton's law of cooling;

$$\frac{dT_s}{dt} = -k(T_s - T_f) \quad \text{Eq. 4. 1. 1}$$

where $T_s = T_s(t)$ and $T_f = 0$ is the temperature of the wing leading edge surface and heating fabric, respectively, k is the heat transfer coefficient of the fiberglass composite

(in $[W * m^{-1} * ^\circ C]$), and the over dot denotes a derivative in time. Since the wing surface is being heated up and $T_s < T_f$ during meso-time scales, $\frac{dT_s}{dt} > 0$ by Equation 4.1.1. For the wing's surface initial temperature of $T_s(0) = T_i$ (where T_i is the temperature of the iced edge), the particular solution of Eq. 4. 1. 1 is;

$$T_s(t) = T_f + (T_i - T_f)e^{-kt} \quad \text{Eq. 4. 1. 2}$$

such that after a given relaxation period (i.e. $t \rightarrow \infty$), the system attains thermodynamic equilibrium (i.e. $T_s \rightarrow T_f$).

4.2. OHM's Law

The resistance is an inherent quality of the Hi-Carbon heating system and the theoretical independent to the applied voltage and flowing current. It is primarily dependent of the fabric's temperature and geometry;

$$R = \rho \frac{L}{A} \quad \text{Eq. 4. 2. 1}$$

where L is the length of the conductor, A is the cross-sectional area of the conductor, and ρ is electrical resistivity.

Furthermore, there is a known relationship between the resistance of a material and the temperature; resistance is directly proportional to temperature via the temperature coefficient of resistivity α ;

$$R = R_0[1 + \alpha(T - T_0)] \quad \text{Eq. 4. 2. 2}$$

$$\alpha_T = \frac{100}{R_T} \cdot \frac{dR}{dT} \quad \text{Eq. 4. 2. 3}$$

where R_0 is the initial resistance value, T_0 is the initial temperature value corresponding to R_0 and T is the temperature corresponding to $R = R(T)$.

Moreover, Ohm's law, given by Eq. 4. 2. 1, simplifies the relation between current and the dissipated thermal energy of the system the power, P , (in $1 W = 1 J \cdot s^{-1}$). For DC, the rate of energy loss via resistive heating is quadratically proportional to voltage for a constant resistance such that $I = \frac{V}{R}$ gives:

$$P = I^2 \cdot R \quad \text{Eq. 4. 2. 4}$$

or in terms of the current density J and electric field E :

$$P = J \cdot E \quad \text{Eq. 4. 2. 5}$$

Similarly, for AC, the power is often denoted as the average power P_{avg} via the circuit power factor $\cos(\theta)$;

$$P_{avg} = V \cdot I \cdot \cos(\theta) \quad \text{Eq. 4. 2. 6}$$

where V and I are the root-mean-square (rms) voltage and current values, respectively, separated by a phase angle θ .

4.3. Joule Heating

The fundamental mechanism enabling the carbon fiber fabric to de-ice the leading edge of an aircraft wing is that of Joule heating. Also known as Ohmic heating and

resistive heating, Joule heating relies on the collisions of charge carriers (typically electrons) with the ionic lattice constituting the conductive material. As an applied voltage acts to move charges in an owing current, the inherent resistance of the heating system is produced by the collisions of electrons with carbon atoms. As a result, kinetic energy is lost by the owing charges and dissipated as thermal energy. The heat is transferred through the fiberglass (as it is in thermal contact with the Hi-Carbon fabric) such that the leading edge of the wing may increase in temperature and ice buildup may be melted.

The dissipated thermal energy Q in J, at a given time of an electrical conductor of constant resistance is quadratically proportional to the current flowing through it, as expressed in the following it;

$$Q \propto I^2 \quad \text{Eq. 4. 3. 1}$$

such that Q at a given time, dissipated by a conductor with constant current is linearly proportional to the conductor's resistance according to the equation expressed below:

$$Q \propto R \quad \text{Eq. 4. 3. 2}$$

Joule's Law expresses that the thermal energy which disseminates from a conductor with constant R and I are linearly proportional to the time (t) that the current flows through it:

$$Q \propto t \quad \text{Eq. 4. 3. 3}$$

Using the Eq. 4. 3. 1, Eq. 4. 3. 2 and Eq. 4. 3. 3 give;

$$Q = J^{-1} \cdot I^2 \cdot R \cdot t \quad \text{Eq. 4. 3. 4}$$

where $j = 0$ is Joule's mechanical equivalent of heat defined as the amount of mechanical energy that yields a single unit of heat.

4.4. Self-Heating Effects

The electrical power input to the Hi-Carbon heating source is just the basic equation from Eq. 2. 3. 4:

$$P_E = V \cdot I = I^2 \cdot R = \frac{V^2}{R} \quad \text{Eq. 2. 3. 4}$$

By Joule's Law, the thermal energy is proportional to the square of the current and the resistance. The thermal energy in respect to time is thermal energy generation, therefore, thermal energy generation can be written as:

$$\dot{E} = I^2 \cdot R = \left(\frac{V}{R}\right)^2 \cdot R = \frac{V^2}{R} \quad \text{Eq. 4. 4. 1}$$

As shown in Eq. 4. 4. 1 and Eq. 2. 3. 4, the thermal energy generation is proportional to the electrical power as:

$$\dot{E} = P_E \quad \text{Eq. 4. 4. 2}$$

According to the first law of thermodynamics, work done can be rewritten as;

$$W = m \cdot C_p \cdot \frac{dT}{dt} \quad \text{Eq. 4. 4. 3}$$

$$m \cdot C_p \cdot \frac{dT}{dt} = \dot{q}_g - \dot{q}_c \quad \text{Eq. 4. 4. 4}$$

where \dot{q}_g is the heat generated and \dot{q}_c is the energy given off. The energy lost, we can write the equation as;

$$\dot{q}_c = \delta \cdot \Delta T \quad \text{Eq. 4. 4. 5}$$

where δ is the dissipation constant. Substituting Joule's law to convection heat transfer as (Moran, Shapiro, Boettner, & Bailey, 2011):

$$m \cdot C_p \cdot \frac{dT}{dt} = \frac{V^2}{R} - \delta \cdot (T - T_0) \quad \text{Eq. 4. 4. 6}$$

- m : Mass of the material
- C_p : Specific heat of the material
- T : Material temperature
- T_0 : Ambient temperature

Also Eq. 4. 4. 6 can be simplified by mass multiple with specific heat

$$C \cdot \frac{dT}{dt} = \frac{V^2}{R} - \delta \cdot (T - T_0) \quad \text{Eq. 4. 4. 7}$$

where C is the heat capacity and above equation can be re-write as the self-heating equation as;

$$\frac{dH}{dt} = \frac{dH_L}{dt} + \frac{dH_A}{dt} \quad \text{Eq. 4. 4. 8}$$

where

$$\frac{dH}{dt} = \frac{V^2}{R(T)} \quad \text{Eq. 4. 4. 9}$$

$$\frac{dH_L}{dt} = \delta \cdot (T - T_0) \quad \text{Eq. 4. 4. 10}$$

$$\frac{dH_A}{dt} = C \cdot \frac{dT}{dt} \quad \text{Eq. 4. 4. 11}$$

where first equation is the rate of stored thermal energy supplied, second equation is the rate of energy loss and last equation is the rate of energy absorbed. The resistance is proportional to the temperature, and using the first order ordinary differential equation, Eq. 4. 4. 6 can be simplified to;

$$\frac{dT}{dt} + k \cdot T(t) = x(t) \quad \text{Eq. 4. 4. 12}$$

where

$$k = \frac{\delta}{C} \quad \text{Eq. 4. 4. 13}$$

$$x(t) = \left(\frac{V^2}{R(T)} + \delta \cdot T_0 \right) \cdot \left(\frac{1}{C} \right) \quad \text{Eq. 4. 4. 14}$$

where δ is the dissipation constant. It is can be defined by change in power dissipation over change in the temperature. The above differential equation (Eq. 4. 4. 12) gives a new equation as;

$$T(t) = e^{-k \cdot t} \cdot \left(\frac{x(t)}{k} \cdot e^{kt} + \left(T_0 - \frac{x(t)}{k} \right) \right) \quad \text{Eq. 4. 4. 15}$$

And when the temperature in respect to time is zero, we can derive another equation from Newton's law of cooling:

$$P_T = \frac{dH_L}{dt} = \delta \cdot (T - T_0) \quad \text{Eq. 4. 4. 16}$$

- P_T : The rate of heat transferred

With Eq. 4. 4. 16, the heat-transfer coefficient and exposed surface area are constant and temperature T is a function of resistor R , and $T_0 = T_i$, which is initial temperature. Therefore, Eq. 4. 4. 16 can be rewritten as;

$$P_T = \delta \cdot (T_{(R)} - T_i) \quad \text{Eq. 4. 4. 17}$$

In order to achieve equilibrium, the Eq. 2. 3. 4 and Eq. 4. 4. 17 rates have to be equal.

$$P_E = P_T \quad \text{Eq. 4. 4. 18}$$

$$V \cdot I = \delta \cdot (T_{(R)} - T_i) \quad \text{Eq. 4. 4. 19}$$

As mentioned in Ohm's law, current is voltage over resistor $\left(\frac{V}{R}\right)$, but current varies with the resistor ($I_{(R)}$), and the resistor varies with temperature ($R_{(T)}$). So with Ohm's law and Eq. 4. 4. 19, the temperature of Hi-Carbon as a function of the resistance equation is:

$$T_{(R)} = T_i + \frac{V^2}{\delta \cdot R_{(T)}} \quad \text{Eq. 4. 4. 20}$$

The Hi-Carbon heating source is acting as a negative temperature coefficient (NTC) thermistor. NTC is when the resistance decreases and the temperature increases.

NTC thermistors can be described with the following sensitivity index (β parameter) equation:

$$R = A \cdot e^{\frac{\beta}{T}} \quad \text{Eq. 4. 4. 21}$$

- R : Thermistor resistance at temperature T
- A : Constant of equation
- β : Material constant
- T : Thermistor temperature in Kelvin (K)

For the given temperature range to calculate beta, the equation of beta is expressed below:

$$\beta = \left(\frac{T_1 \cdot T_2}{T_2 - T_1} \right) \cdot \ln \left(\frac{R_1}{R_2} \right) \quad \text{Eq. 4. 4. 22}$$

To calculate the temperature coefficient (α) is the slope of the curve at a given point,

$$\alpha = \frac{100}{R} \cdot \frac{dR}{dT} \quad \text{Eq. 4. 4. 23}$$

The relationship between the temperature coefficient and the beta can drive by substituting the Eq. 4. 4. 21 into the Eq. 4. 4. 23. So the temperature coefficient can be rewritten as,

$$\alpha = -\frac{\beta}{T^2} \quad \text{Eq. 4. 4. 24}$$

The best representation of the resistance versus temperature of the NTC thermistor is the Steinhart-Hart thermistor equation. It is a polynomial base formula. The Steinhart-Hart thermistor equation gives more accurate result of resistance versus

temperature with greater range of temperature than the beta parameter equation. To calculate the temperature with known resistance, it can be expressed as:

$$\frac{1}{T} = a + b \cdot \ln(R) + c \cdot (\ln(R))^3 \quad \text{Eq. 4. 4. 25}$$

To calculate the resistance with known temperature, the formula can be rearranged as;

$$R = e^{\left[\left(-\frac{\chi}{2} + \left(\frac{\chi^2}{4} + \frac{\psi^3}{27} \right)^{\frac{1}{2}} \right)^{\frac{1}{3}} + \left(-\frac{\chi}{2} - \left(\frac{\chi^2}{4} + \frac{\psi^3}{27} \right)^{\frac{1}{2}} \right)^{\frac{1}{3}} \right]} \quad \text{Eq. 4. 4. 26}$$

where:

$$\chi = \frac{a-1}{T \cdot c}$$

$$\psi = \frac{b}{c}$$

The a , b and c are the constant values and the formula can be calculated with three sets of temperatures: the low end, middle and high ends. The temperature error for the Steinhart-Hart equation is about ± 0.001 °C over a 100 °C temperature span. Also similarly, a , b and c can be determined from the experiment and that constants values substituted into the Eq. 4. 4. 25.

4.5. Thermal Time Constant

“The Thermal Time Constant is a measurement of the time required for the thermistor to respond to a change in the ambient temperature. The technical definition of Thermal Time Constant is, the time required for a thermistor to change 63.2% of the total

difference between its initial and final body temperature when subjected to a step function change in temperature, under zero power conditions” (Thermal Time Constant, 2012).

The 63.2% is not a random number; it is derived from the behavior of exponential function. For example, to calculate the RC circuit’s time constant while the capacitor is charging, the equation can be expressed as below:

$$\tau = -R \cdot C \cdot \ln\left(1 - \frac{V_o}{V_{in}}\right) \quad \text{Eq. 4. 5. 1}$$

- τ : Time constant
- C : Capacitor
- V_o : Output voltage
- V_{in} : Input voltage

In the series RC circuit, the time constant can be expressed as:

$$\tau = R \cdot C \quad \text{Eq. 4. 5. 2}$$

To make the thermal time constant same, Eq. 4. 5. 1 and Eq. 4. 5. 2 have to be in equilibrium. Therefore, the equation “ $\ln\left(1 - \frac{V_o}{V_{in}}\right)$ ” has to be equal to negative one. So deriving the equilibrium equation between the Eq. 4. 5. 1 and Eq. 4. 5. 2:

$$\ln\left(1 - \frac{V_o}{V_i}\right) = -1$$

$$1 - \frac{V_o}{V_i} = e^{-1}$$

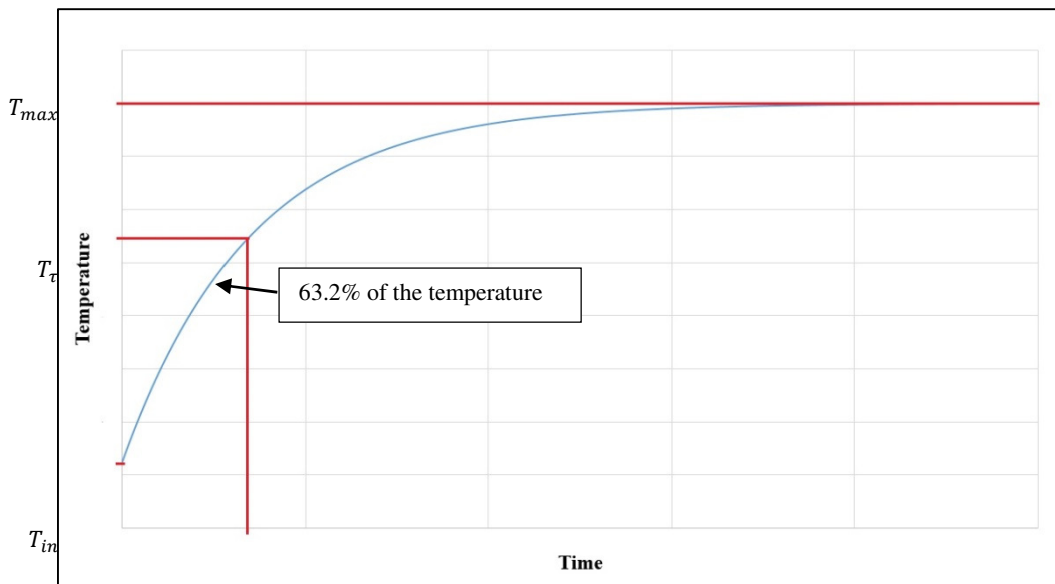
$$\frac{V_o}{V_i} = 1 - e^{-1}$$

$$\frac{V_o}{V_i} \approx 0.632$$

The purpose for calculating the thermal time constant is to determine the temperature of the thermal time constant and the temperature value that correspond to the resistance for the thermal time constant that will correspond to 63.2% of the resistance span. The equation to calculate the temperature at the thermal constant time is:

$$T_\tau = 0.632(T_{max} - T_i) + T_i \quad \text{Eq. 4. 5. 3}$$

For a visualization of the thermal constant time temperature, see Figure 21 below:



τ

Figure 21. Thermal constant time

By using the Steinhart-Hart equation (Eq. 4. 4. 25) or other approximation equation (Eq. 4. 4. 21), the resistance at the thermal constant time can be calculated. But the thermal constant time can be affected by the mass of the resistor, mounting, environment, and other factors.

4.6. Heat Transfer

4.6.1. Thermal Conductivity

For the composite material, there is more than one component. Composites can be classified as isotropic, anisotropic or orthotropic material. The thermal conductivity components for one-dimensional composites are relative to volume fraction. When all the fibers are in the unidirectional lay-up, this lay-up called a lamina and it is orthotropic lamina. When the fibers are with various angles lay-up, this lay-up called a laminate and it is anisotropic laminate. Also there is special case as quasi-isotropic lay-up (Campbell, 2010).

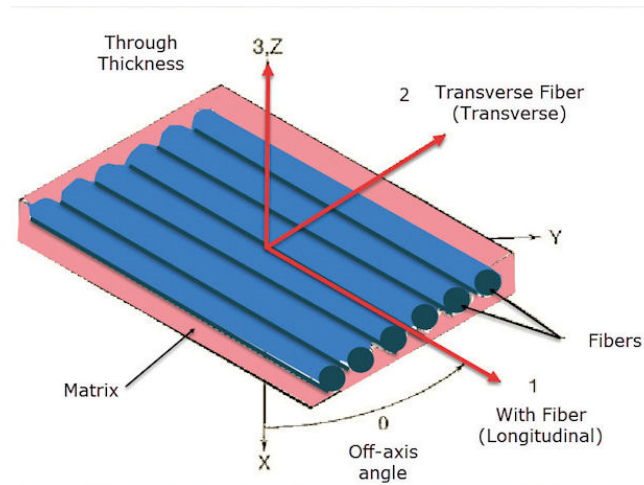


Figure 22. Schematic sketch of composites direction (Abbey, 2014)

In the through the thickness direction (3-direction), heat flow is considerably to be more complex and harder to solve. For the polymer matrix composites, mostly have low thermal conductivity because of the polymeric resins (epoxy resin) act like insulator due

to its stable chemical bonding, composition and structure (Callister, 2003). The thermal conductivity for the fiber direction (1-direction) is (Tavman & Akinici, 2000);

$$k_s = \frac{k_m \cdot k_f}{k_m \cdot V_m + k_f \cdot V_m} \quad \text{Eq. 4. 6. 1}$$

where k_s is the thermal conductivity of 1-direction, k_m is the matrix thermal conductivity, k_f is the fiber thermal conductivity, V_m is the volume of matrix, and V_f is the volume of fiber. And the thermal conductivity for the normal to the fibers is;

$$k_p = k_f \cdot V_f + k_m \cdot V_m \quad \text{Eq. 4. 6. 2}$$

Above two equation (Eq. 4. 6. 1 and Eq. 4. 6. 2) are the simplest calculate the thermal conductivities in the fiber and normal to the fiber direction.

Springer and Tsai developed a square distribution of cylindrical fibers in the matrix material, and the equation of the thermal conductivity in normal to the fiber is;

$$k_p = k_m \left[1 - 2 \cdot \sqrt{\frac{V_f}{\pi}} + \frac{1}{B} \cdot \left(\pi - \frac{4}{\sqrt{1 - \left(B^2 \cdot \frac{V_f}{\pi} \right)}} \cdot \tan^{-1} \left(\frac{\sqrt{1 - \left(B^2 \cdot \frac{V_f}{\pi} \right)}}{1 + B \cdot \sqrt{\frac{V_f}{\pi}}} \right) \right) \right]$$

$$\text{Eq. 4. 6. 3}$$

where,

$$B = 2 \left(\frac{k_m}{k_f} - 1 \right)$$

And there are several equations to derive the thermal conductivity like Rayleigh, Cheng-Vachon, Halpin-Tsai and Lewis-Nielsen. They are all having different conditions to use like shapes of fiber. The equations are showing in below;

Rayleigh equation

$$k_p = k_m \left[1 - \frac{2 \cdot V_f}{\gamma + V_f - \frac{C_1}{\gamma} \cdot V_f^4 - \frac{C_2}{\gamma} V_f^8} \right] \quad \text{Eq. 4. 6. 4}$$

where,

$$C_1 = 0.3058, C_2 = 0.0134, \text{ and } \gamma = \frac{\left(\frac{k_m}{k_f}\right)^{+1}}{\left(\frac{k_m}{k_f}\right)^{-1}}$$

Cheng-Vachon equation

$$\frac{1}{k_p} = \frac{1}{\sqrt{C \cdot (A) \cdot (k_m + B \cdot (-A))}} \cdot \ln \left(\frac{\sqrt{k_m + B \cdot (-A)} + \frac{B}{2} \cdot \sqrt{C \cdot (A)}}{\sqrt{k_m + B \cdot (-A)} - \frac{B}{2} \cdot \sqrt{C \cdot (A)}} \right) + \frac{1 - B}{k_m}$$

Eq. 4. 6. 5

where,

$$A = k_m - k_f, B = \sqrt{\frac{3 \cdot V_f}{2}}, \text{ and } C = -4 \cdot \sqrt{\frac{2}{3 \cdot V_f}}$$

if the thermal conductivity of the matrix is much smaller than the fiber, $k_m \ll k_f$ or $\frac{k_f}{k_m} >$

100, Cheng-Vachon equation can be rewritten as;

$$k_p = \frac{k_m}{1 - B} \quad \text{Eq. 4. 6. 6}$$

Halpin-Tsai equation

$$k_p = k_m \cdot \left[\frac{1 + \zeta \cdot \phi \cdot \eta}{1 - \eta \cdot \phi} \right] \quad \text{Eq. 4. 6. 7}$$

where,

$$\eta = \frac{\left(\frac{k_f}{k_m}\right)^{-1}}{\left(\frac{k_f}{k_m}\right)^{+\zeta}}$$

For the circular or square fibers ζ is equal to one.

Lastly, Lewis-Nielsen equation (Zimmer, et al., 2012)

$$k_p = k_m \left(\frac{1 + A \cdot B \cdot V_f}{1 - B \cdot V_f \cdot \psi} \right) \quad \text{Eq. 4. 6. 8}$$

where, $A = 8.38$, $B = \frac{\left(\frac{k_f}{k_m}\right)^{-1}}{\left(\frac{k_f}{k_m}\right)^{+A}}$, $\psi = 1 + \left(\frac{1 - \psi_m}{\psi_m^2}\right) \cdot V_f$, and $\psi_m = 0.52$

With Eq. 4. 6. 2 through Eq. 4. 6. 8, effective thermal conductivity can be predicting with comparing with different equations for glass fiber reinforced composite materials.

4.6.2. Heat Transfer of Thin Plate

Most polymer reinforced materials are thermally anisotropic and inhomogeneous due to differences of conductivities between the fiber and matrix. By using the thermal laminate theories (TLT) for composite materials (Rolfes, 1990), through thickness temperature distribution for composites plates can be expressed by a linear function when the all layers of the thermal conductivities in the 3-direction are identical, and no heat

transfer resistance at the interfaces (Ozisik, 1968). For an orthotropic nonhomogeneous heat transfer for a multilayer with heat generation governing equation is;

$$\frac{\partial T_i(z, t)}{\partial t} = \alpha_i \cdot \nabla^2 \cdot T_i(z, t) + \frac{\alpha_i}{k_i} \cdot g_i(z, t) \quad \text{Eq. 4. 6. 9}$$

subject to

$$z_i \leq z \leq z_{i+1} , \quad t > 0$$

where,

$$\nabla^2 \equiv \frac{1}{z^p} \cdot \frac{\partial}{\partial z} \cdot \left(z^p \cdot \frac{\partial}{\partial z} \right) \quad \text{Eq. 4. 6. 10}$$

Eq. 4. 6. 10 is the one-dimensional Laplace differential operator; p value for the plate is zero. The i represent i^{th} layer of composites ($i = 1, 2, \dots m$). α is thermal diffusivity and T_i is the temperature of layer i . The Eq. 4. 6. 9 has some assumption:

1. Inside the layer, no heat flux generated
2. Perfectly thermal contact between all layers
3. Heat flows in the 3-direction

For the assumption 3, the system has to be one dimensional heat transfer. Therefore, the temperature distribution has to be uniform. To satisfy that assumption, Biot number has to be less than 0.1. The carbon fabric with composite structure Biot number is greater than 0.1.

$$Biot = \frac{h \cdot L_c}{k} \quad \text{Eq. 4. 6. 11}$$

The initial condition can be expressed with given function $F_i(z)$

$$T_i(z, 0) = F_i(z), \quad z_i \leq z \leq z_{i+1} \quad \text{Eq. 4. 6. 12}$$

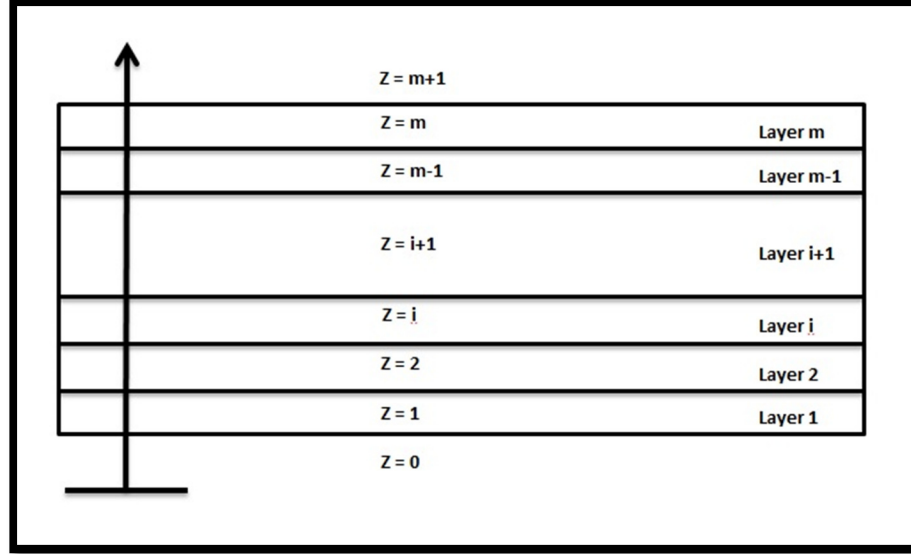


Figure 23 Composite region consisting of m layers

The boundary conditions of inner surface ($z = z_1$), outer surface ($z = z_{m+1}$) and interfaces ($z = z_{i+1}$) are describe as;

$$\frac{\partial T_1(z_1, t)}{\partial z} = 0 \quad \text{Eq. 4. 6. 13}$$

$$T_i(z_{i+1}, t) = T_{i+1}(z_{i+1}, t), \quad z = z_{i+1} \quad \text{Eq. 4. 6. 14}$$

$$k_i \cdot \frac{\partial T_i(z_{i+1}, t)}{\partial z} = k_{i+1} \cdot \frac{\partial T_{i+1}(z_{i+1}, t)}{\partial z}, \quad z = z_{i+1} \quad \text{Eq. 4. 6. 15}$$

$$h \cdot [T_m(z_{m+1}, t) - T_\infty(t)] = -k_m \cdot \frac{\partial T_m(z_{m+1}, t)}{\partial z}, \quad z = z_{m+1} \quad \text{Eq. 4. 6. 16}$$

where h_1 and h_m are the heat transfer coefficients at the inner and outer surface, and in this section i for the thermal conductivity is representing the layers, the coordinates of the layers show in Figure 23.

Antonopoulos and Tzivanidis (Antonopoulos & Tzivanidis, 1995) derived new dependent variable by non-homogeneous problem to homogeneous problem for the two convection boundary condition.

$$\theta_i(z, t) = T_i(z, t) - T_\infty(t), \quad z_i \leq z \leq z_{i+1}, \quad i = 1, 2, \dots, m \quad \text{Eq. 4. 6. 17}$$

Now, the Eq. 4. 6. 9 becomes;

$$\frac{\partial \theta_i(z, t)}{\partial t} = \alpha_i \cdot \nabla^2 \cdot \theta_i(z, t) + \frac{\alpha_i}{k_i} \cdot g_i(z, t) - \frac{dT_\infty(z, t)}{dt} \quad \text{Eq. 4. 6. 18}$$

and the boundary conditions become;

$$\frac{\partial \theta_1(z_1, t)}{\partial z} = 0 \quad \text{Eq. 4. 6. 19}$$

$$\theta_i(z_{i+1}, t) = \theta_{i+1}(z_{i+1}, t) \quad \text{Eq. 4. 6. 20}$$

$$k_i \cdot \frac{\partial \theta_i(z_{i+1}, t)}{\partial z} - k_{i+1} \cdot \frac{\partial \theta_{i+1}(z_{i+1}, t)}{\partial z} = 0 \quad \text{Eq. 4. 6. 21}$$

$$k_m \cdot \frac{\partial \theta_m(z_{m+1}, t)}{\partial z} + h_m \cdot \theta_m(z_{m+1}, t) = 0 \quad \text{Eq. 4. 6. 22}$$

also, the initial condition becomes

$$\theta_i(z, 0) = F_i(z) - T_\infty(0) \equiv f_i(z), \quad z_i \leq z \leq z_{i+1} \quad \text{Eq. 4. 6. 23}$$

By assuming separation of variables, the $\theta_i(z, t)$ can be expressed as;

$$\theta_i(z, t) = \sum_{n=1}^{\infty} Z_{in}(z) \cdot \Gamma_n(t) , \quad z_i \leq z \leq z_{i+1} \quad \text{Eq. 4. 6. 24}$$

with $i = 1, 2, \dots, m$, and the function of Z_{in} and Γ_n can be determine by following the summation from the fundamental theorem. When substitute the general form of the $T(z, t)$ into the Eq. 4. 6. 9,

$$\alpha \cdot \frac{\nabla^2 Z(z)}{Z(z)} = \frac{\dot{\Gamma}(t)}{\Gamma(t)} \quad \text{Eq. 4. 6. 25}$$

where $\dot{\Gamma}$ is the derivative of temperature respect to time. And it is only true when some constant ($-\beta^2$) equal to both side of Eq. 4. 6. 25. Eigen function Z_{in} has to satisfy the eigenvalue problem as shown in below for i layers with n series.

$$\alpha_i \cdot \nabla^2 \cdot Z_{in}(z) + \beta_n^2 \cdot Z_{in}(z) = 0 , \quad z_i \leq z \leq z_{i+1} \quad \text{Eq. 4. 6. 26}$$

where ∇^2 is defined by Eq. 4. 6. 10 and with the boundary conditions

$$\frac{dZ_{1n}(z_1)}{dz} = 0 \quad \text{Eq. 4. 6. 27}$$

$$Z_{in}(z_{i+1}) = Z_{i+1,n}(z_{i+1}) \quad \text{Eq. 4. 6. 28}$$

$$k_i \cdot \frac{dZ_{in}(z_{i+1})}{dz} = k_{i+1} \cdot \frac{dZ_{i+1,n}(z_{i+1})}{dz} \quad \text{Eq. 4. 6. 29}$$

$$k_m \cdot \frac{dZ_{mn}(z_{m+1})}{dz} + h \cdot Z_{mn}(z_{m+1}) = 0 \quad \text{Eq. 4. 6. 30}$$

Above Eq. 4. 6. 26 eigenvalue problem can be solve by

$$Z_{in}(z) = C_{in} \cdot \Phi_{in}(z) + D_{in} \cdot \Psi_{in}(z) , \quad z_i \leq z \leq z_{i+1} \quad \text{Eq. 4. 6. 31}$$

The functions Φ and Ψ are linearly independent solutions of Eq. 4. 6. 26.

Table 2. The linearly independent solutions (Ozsisik, 1968)

Geometry	$\Phi_{in}(z)$	$\Psi_{in}(z)$
Plate	$\cos\left(\frac{\beta_{in}}{\sqrt{\alpha_i}} \cdot z\right)$	$\sin\left(\frac{\beta_{in}}{\sqrt{\alpha_i}} \cdot z\right)$
Cylinder	$J_0\left(\frac{\beta_{in}}{\sqrt{\alpha_i}} \cdot z\right)$	$Y_0\left(\frac{\beta_{in}}{\sqrt{\alpha_i}} \cdot z\right)$
Sphere	$\frac{1}{z} \cdot \sin\left(\frac{\beta_{in}}{\sqrt{\alpha_i}} \cdot z\right)$	$\frac{1}{z} \cdot \cos\left(\frac{\beta_{in}}{\sqrt{\alpha_i}} \cdot z\right)$

by substituting the functions Φ and Ψ into the Eq. 4. 6. 31 and then apply to the boundary conditions Eq. 4. 6. 27 to Eq. 4. 6. 30, constant values C_{in} and D_{in} can be determined. The boundary conditions can be re-write as;

$$C_{1n} \cdot \phi'_{1n}(z_1) + D_{1n} \cdot \psi'_{1n}(z_1) = 0 \quad \text{Eq. 4. 6. 32}$$

$$\Phi_{in}(z_{i+1}) \cdot C_{in} + \Psi_{in}(z_{i+1}) \cdot D_{in} - \Phi_{i+1,n}(z_{i+1}) \cdot C_{i+1,n} - \Psi_{i+1,n}(z_{i+1}) \cdot D_{i+1,n} = 0$$

$$\text{Eq. 4. 6. 33}$$

$$k_i \cdot \Phi'_{in}(z_{i+1}) \cdot C_{in} + k_i \cdot \Psi_{in}(z_{i+1}) \cdot D_{in} - k_{i+1} \cdot \Phi'_{i+1,n}(z_{i+1}) \cdot C_{i+1,n} - k_{i+1} \cdot \Psi'_{i+1,n}(z_{i+1}) \cdot D_{i+1,n} = 0$$

$$\text{Eq. 4. 6. 34}$$

$$[h \cdot \Phi_{mn}(z_{m+1}) + k_m \cdot \Phi'_{mn}(z_{m+1})] \cdot C_{mn} + [h \cdot \Psi_{mn}(z_{m+1}) + k_m \cdot \Psi'_{mn}(z_{m+1})] \cdot D_{mn} = 0$$

$$\text{Eq. 4. 6. 35}$$

with $i = 1, 2, \dots, m - 1$ and Φ' and Ψ' are derivatives with respect to z . Above four equations can be re-write as matrix form. Following the Cramer's theorem, these homogeneous equations only have non-trivial solutions when the determinant of matrix is

zero. The homogeneous set of $2 \cdot m$ eigenvalues can be using for determine the unknown constant C and D , where one of the constant have to be determined arbitrarily.

Next step is calculation of the solution of the time component. To determine the solution of the time component, it requires the $g_i(z, t)$ variables and initial condition.

$$f_i(z) = \sum_{n=1}^{\infty} f_n^* \cdot Z_{in}(z) \quad \text{Eq. 4. 6. 36}$$

$$\frac{\alpha_i}{k_i} g_i(z, t) = \sum_{n=1}^{\infty} g_n^*(t) \cdot Z_{in}(z) \quad \text{Eq. 4. 6. 37}$$

$$1 = \sum_{n=1}^{\infty} I_n^*(t) \cdot Z_{in}(z) \quad \text{Eq. 4. 6. 38}$$

where $i = 1, 2, \dots, m$. The Eq. 4. 6. 36 to Eq. 4. 6. 38 are representing by the Fourier series, due to that the appropriate variable of space and time has to contain. The unknown Fourier constants are expressed as;

$$f_i^*(z) = \frac{\sum_{i=1}^m \frac{k_i}{\alpha_i} \cdot \int_{z_i}^{z_{i+1}} f_i(z) \cdot Z_{in}(z) \cdot z^p dx}{N} \quad \text{Eq. 4. 6. 39}$$

$$g_n^*(t) = \frac{\sum_{i=1}^m \frac{k_i}{\alpha_i} \cdot \int_{z_i}^{z_{i+1}} g_i(z, t) \cdot Z_{in}(z) \cdot z^p dx}{N} \quad \text{Eq. 4. 6. 40}$$

$$I_n^*(t) = \frac{\sum_{i=1}^m \frac{k_i}{\alpha_i} \cdot \int_{z_i}^{z_{i+1}} Z_{in}(z) \cdot z^p dx}{N} \quad \text{Eq. 4. 6. 41}$$

where,

$$N = \sum_{i=1}^m \frac{k_i}{\alpha_i} \cdot \int_{z_i}^{z_{i+1}} Z_{in}^2(z) \cdot z^p dz \quad \text{Eq. 4. 6. 42}$$

To determine the values of Fourier constants use the orthogonality property of the Eigen functions over an individual layer. Before determine, at the both side are multiplied by $\frac{k_i}{\alpha_i} \cdot Z_{in'} \cdot z^p$, then integrated by individual layer and summation over all layers. For example,

$$\sum_{i=1}^m \frac{k_i}{\alpha_i} \cdot \int_{z_i}^{z_{i+1}} f_i(z) \cdot Z_{in'} \cdot z^p dz = \sum_{i=1}^m \sum_{n=1}^{\infty} f_n^* \cdot \frac{k_i}{\alpha_i} \cdot \int_{z_i}^{z_{i+1}} Z_{in}(z) \cdot Z_{in'}(z) \cdot z^p dz \quad \text{Eq. 4. 6. 43}$$

And orthogonality is defined as;

$$\int_R Z_n(z) \cdot Z_{n'}(z) dz = \begin{cases} 0 & \text{for } n \neq n' \\ \text{const.} & \text{for } n = n' \end{cases} \quad \text{Eq. 4. 6. 44}$$

With above condition, the Eq. 4. 6. 43 can be rearranging as;

$$\sum_{i=1}^m \frac{k_i}{\alpha_i} \cdot \int_{z_i}^{z_{i+1}} f_i(z) \cdot Z_{in} \cdot z^p dz = f_n^* \cdot \sum_{i=1}^m \frac{k_i}{\alpha_i} \cdot \int_{z_i}^{z_{i+1}} Z_{in}^2(z) \cdot z^p dz \quad \text{Eq. 4. 6. 45}$$

The Eq. 4. 6. 37 and Eq. 4. 6. 38 can be rearranging as above;

$$\sum_{i=1}^m \frac{k_i}{\alpha_i} \cdot \int_{z_i}^{z_{i+1}} g_i(z, t) \cdot Z_{in} \cdot z^p dz = V_m^* \cdot \sum_{n=1}^{\infty} \frac{k_i}{\alpha_i} \int_{z_i}^{z_{i+1}} Z_{in}^2(z) \cdot z^p dz \quad \text{Eq. 4. 6. 46}$$

$$\sum_{i=1}^m k_i \cdot \int_{z_i}^{z_{i+1}} g_i(z, t) \cdot Z_{in} \cdot z^p dz = I_n^* \cdot \sum_{i=1}^m k_i \int_{z_i}^{z_{i+1}} Z_{in}^2(z) \cdot z^p dz \quad \text{Eq. 4. 6. 47}$$

The heat transfer Eq. 4. 6. 18 can be rewritten by substitution of Eq. 4. 6. 24, Eq. 4. 6. 37 and Eq. 4. 6. 38 as;

$$\sum_{n=1}^{\infty} \frac{d\Gamma_n(t)}{dt} \cdot Z_{in}(z) = \sum_{n=1}^{\infty} \alpha_i \cdot \Gamma_n(t) \cdot \nabla^2 \cdot Z_{in}(z) + \sum_{n=1}^{\infty} I_n^*(t) \cdot Z_{in}(z) - \sum_{n=1}^{\infty} g_n^*(t) \cdot Z_{in}(z) \quad \text{Eq. 4. 6. 48}$$

Putting the equation From Eq. 4. 6. 26 into the Eq. 4. 6. 48, it can be rewritten with the eigenvalues β_n as;

$$\sum_{n=1}^{\infty} \left[\frac{d\Gamma_n(t)}{dt} + \beta_n^2 \cdot \Gamma_n(t) - g_n^*(t) + I_n^* \cdot \frac{dT_s(t)}{dt} \right] \cdot Z_{in}(z) = 0 \quad \text{Eq. 4. 6. 49}$$

To make above equation to zero, the equation inside of square bracket or Z_{in} has to be zero, but Z_{in} cannot be zero, therefore, inside of the square bracket equation has to be zero. And with that equation, Γ_n can be obtained by using the initial condition,

$$\Gamma_n(t) = e^{-\beta_n^2 t} \cdot \left[\int_0^t \left(g_n^*(t) - I_n^* \cdot \frac{dT_{\infty}(t)}{dt} \right) \cdot e^{\beta_n^2 t} dt + f_n^* \right], \quad \text{for } i = 1 \text{ and } i = m \quad \text{Eq. 4. 6. 50}$$

The external boundaries I_n^* and g_n^* are only valid when $i = 1$ and $i = m$, so between the layers, the external boundaries are zero. Therefore, new $\Gamma_n(t)$ equation obtains by simplifying the inside of the square bracket equation of Eq. 4. 6. 49 as;

$$\Gamma_n(t) = f_n^* \cdot e^{-\beta_n^2 t}, \quad \text{for } i = 2, 3, \dots, m - 1 \quad \text{Eq. 4. 6. 51}$$

The general form of the separation of the variables (Eq. 4. 6. 24) is used to obtain the final expressions of θ_i for each end layers and in between end layers as following equations,

For $i = 1, 2, 3, \dots, m$

$$\theta_i(z, t) = \sum_{n=1}^{\infty} Z_{in}(z) \cdot e^{-\beta_n^2 \cdot t} \cdot \left[\int_0^t \left(g_n^*(t) - I_n^* \cdot \frac{dT(t)}{dt} \right) \cdot e^{\beta_n^2 \cdot t} dt + f_n^* \right] \quad \text{Eq. 4. 6. 52}$$

The temperature at any layers and time can be solving by using above equations with Eq. 4. 6. 17. This heat transfer equation presents solving the layer wise temperature change over the time.

4.7. Prepreg Fiber Glass Calculations

When specifications of the reinforced fiber composite materials is unknown, there is way to calculation the predict values, which is the cured ply thickness equation, by using the Eq. 4. 7. 1, the volume fraction can be obtaining also it makes predicting material.

$$CPT = \frac{wf}{\rho \cdot 10 \cdot V_f} \quad \text{Eq. 4. 7. 1}$$

- wf : Fiber areal weight (g/m^2)
- ρ : Fiber density (g/cm^3)

Chapter V: Experimental Analysis

In this chapter, two different prototypes were examined with three different input voltages. Each proto type had different number of carbon fabric layers, first proto type had five layers and second proto type had ten layers. On top of the carbon fabric, nine layers of fiberglass surface skin will pile up and study about heat transfer through the thickness of each layers of surface skin.

5.1. Methodology

Despite the stated Hi-Carbon manufacturing specifications, upon laboratory experimentation, a single 63.5 by 12.7 centimeter fabric layer failed to reach the target temperature of 38°C within one minute. The cause of this problem was rooted in the manufacturing process of the Hi-Carbon fabric.



Figure 24. Carbon black present in Hi-Carbon (Wikipedia, 2015)

The fundamental resistive component of the Hi-Carbon fabric is a material called carbon black which is shown in Figure 24. Made by the incomplete combustion of heavy petroleum products, carbon black (also known as acetylene black, channel black, furnace black, lamp black, and thermal black) is a type of amorphous carbon allotrope with a high surface area to volume ratio commonly used in diesel oxidation experiments (Arnal, Alzueta, Millera, & Bibao, 2011).

In 2002, the Mitsubishi Chemical Corporation invented a resin-coated carbon black with a high volume resistivity of $\rho \approx 100\Omega \cdot cm$. The intent of the application was to insulate black spacers of optical color filters in color televisions, cameras and other such commodities (Hisashi, Arata, & Sekine, 2002). Although carbon black has thermal, electric and chemical properties similar to the chemically modified grapheme analogue called thermally reduced grapheme oxide (TRGO), it is cheaper and more readily fabricated (Wong, Ambrosi, & Pumera, 2012).

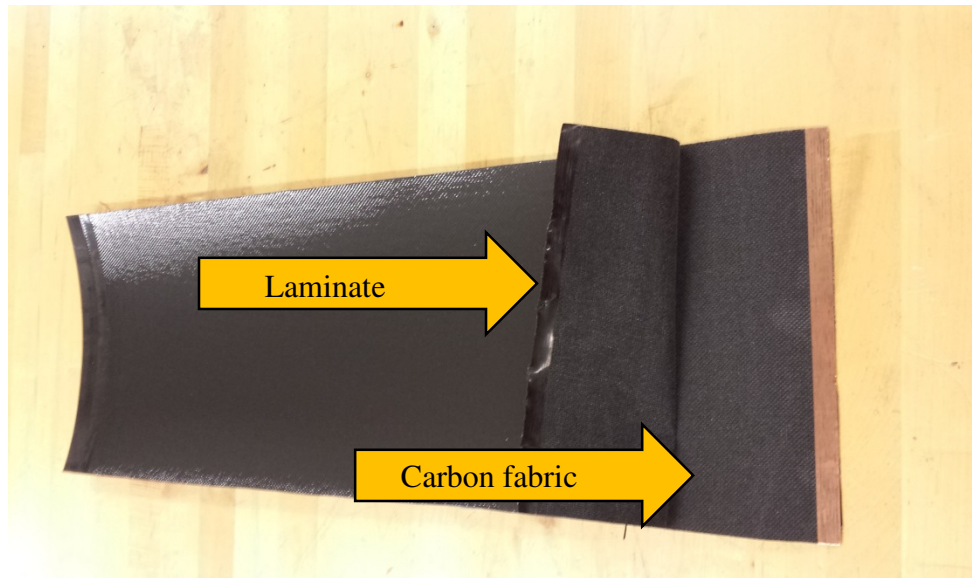


Figure 25. Delaminated Hi-Carbon material

Due to the negative temperature coefficient (NTC) of resistivity of carbon black (see Self-Heating Effects in section 4.4.), the delaminated Hi-Carbon fabric heating rate was not as expected, as the vulnerable carbon black content decreased with delamination. The delaminated fabric is shown in Figure 25. As a result, the temperature change by a measured 7.44 W power supply was insufficient due to the resistance increase from the initial value of approximately 2000 Ω .

To decrease the resistance of the fabric, the fabric area was decreased by shortening the length and width. The resulting smaller dimension between conductive copper plates concentrated the power, yet still did not produce the thermal energy required. Subsequently, the resistance was further decreased by folding the fabric five times; the carbon black on the delaminated fabric was concentrated and the system was less resistive at an average of about 145.37 Ω at room temperature (25°C).

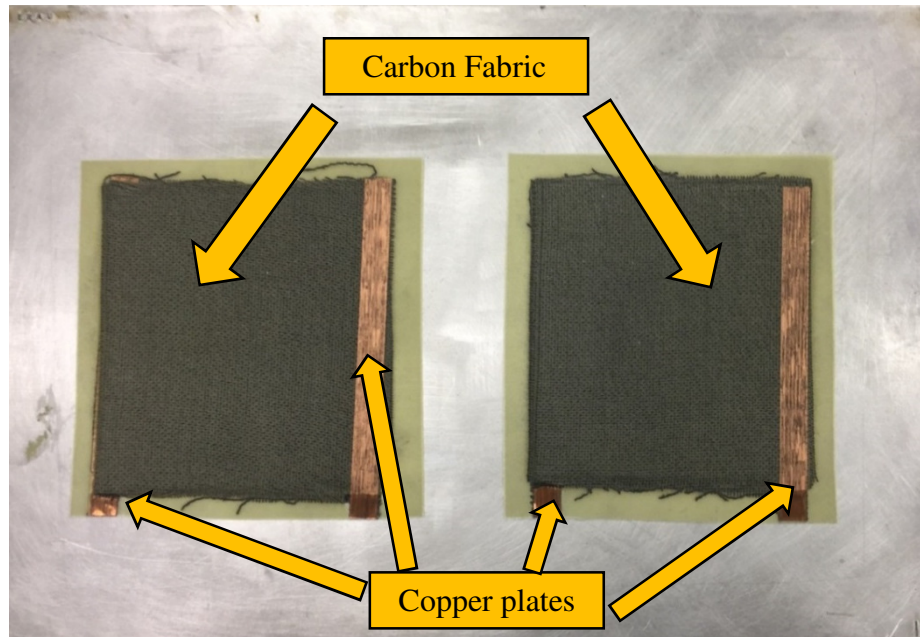


Figure 26. Laminated Hi-Carbon with glass fiber layers with copper conductive plates.

With such modifications, the fabric was able to produce the temperature changes required. The resulting folded delaminated fabric with conductive copper plates measured 5 centimeters in length and width with 2.25 mm in thickness as shown in Figure 26. It is noted that the folds were of odd integers such that the current is evenly distributed between the plates. To further increase the conductance, theoretically, more carbon black could be concentrated.

5.2. Experimental Design

During the composite curing procedure, shown in Figure 27, the fabric layers were compressed by a vacuum system in 260°F oven for 90 minutes followed by a 30

minute cool down. The completed prototypes of the carbon fabric heating systems are shown in Figure 26.



Figure 27. Vacuum compressed proto types in 260 degree oven

Once connected to a power supply, the temperature was measured by a signal box and time was measured by LabVIEW (for accuracy), while attached thermal couples on the prototype surfaces sent data that was digitally displayed by LabVIEW computer software as shown in Figure 28

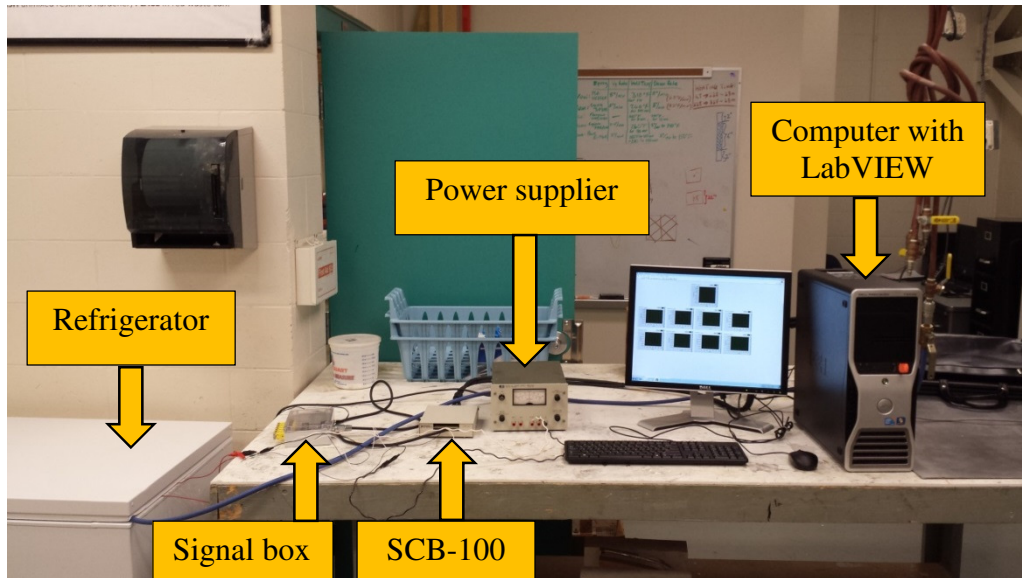


Figure 28. Experimental set-up

Nine layers of the fiberglass consider as wing surface skin and these layers are piled up on top of the carbon fabric heating system. A thermocouple is located at the heat source, and three more thermocouples are located third, sixth and ninth layer of the fiberglass. A vacuum bag was used to hold the fiberglass layers and carbon fabric together as one uniform body, as shown in Figure 29.

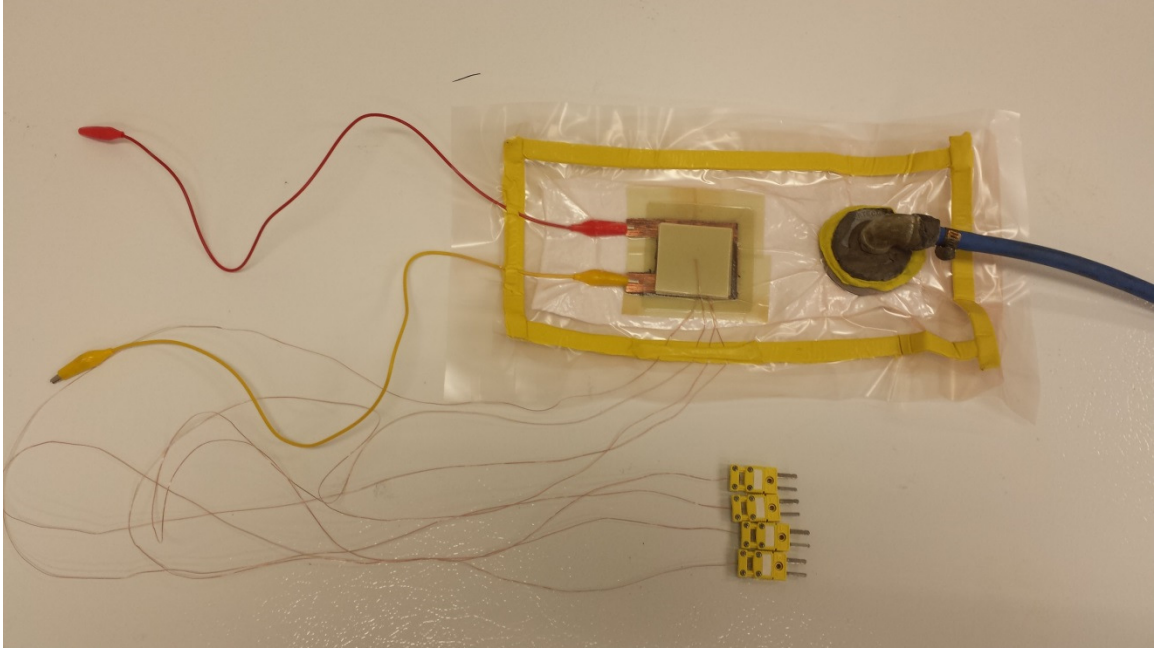


Figure 29. Vacuum bag used to hold the carbon fabric, fiberglass layers and thermocouples together

As shown in Figure 29, red and yellow wire connectors were used to supplying the voltage for the power supplier to the carbon fabric. Four thin wires connected the thermocouples to the signal box. Each of the thermocouples were placed within the carbon fabric layer, third, sixth, and ninth (outer surface) of the fiberglass structure. From the principles of thermocouples in section 3.3.3, each thermocouple will generate a very small voltage due to the temperature different between hot junction and cold junction and these generated voltages will flow into the signal box to be amplified. This signal box (See Figure 30) enables to read the temperature accuracy within $\pm 2^{\circ}\text{C}$.

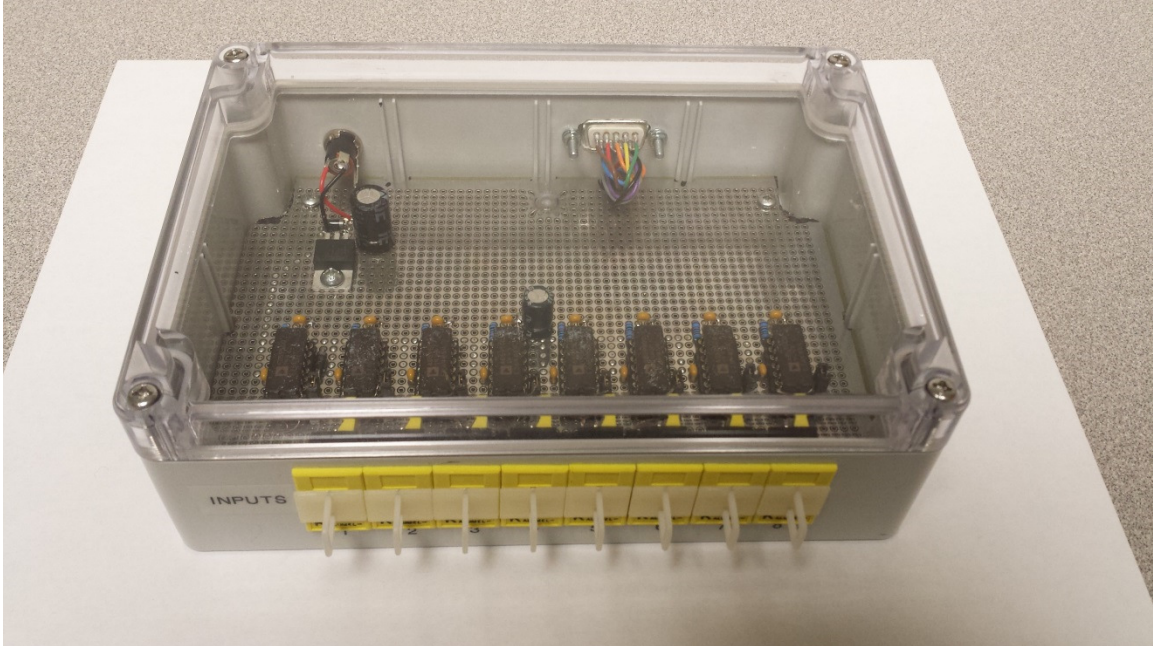


Figure 30. Voltage amplifier for generated voltage from thermocouples

From the signal box, the analog input voltage flowed into the SCB-100. The SCB-100 (See Figure 31) has its own cold-junction compensation temperature sensor for the thermocouple. Data acquisition system converted input analog-to-digital data. The SCB-100 only measures the temperature. It is directly connected to a power supply with one Ohm shunt resistor to measure the current flow to the carbon fabric. In order to measure the accurate current flow without amplifiers, the particular data acquisition needed to be higher than the half Ohms shunt resistor. To get more accurate results and to simplify the calculation, one Ohm shunt resistor is selected in the experiment. The generated voltage and current values are converted to digital signals through the data acquisition system.



Figure 31. NI SCB-100 data acquisition (NI Corp.)

De-icing systems are usually operated at environmental temperatures that below 0°C. In order to simulate such an environment, the carbon fabric de-icing system was tested by installing the prototypes in a refrigerator (See Figure 32).

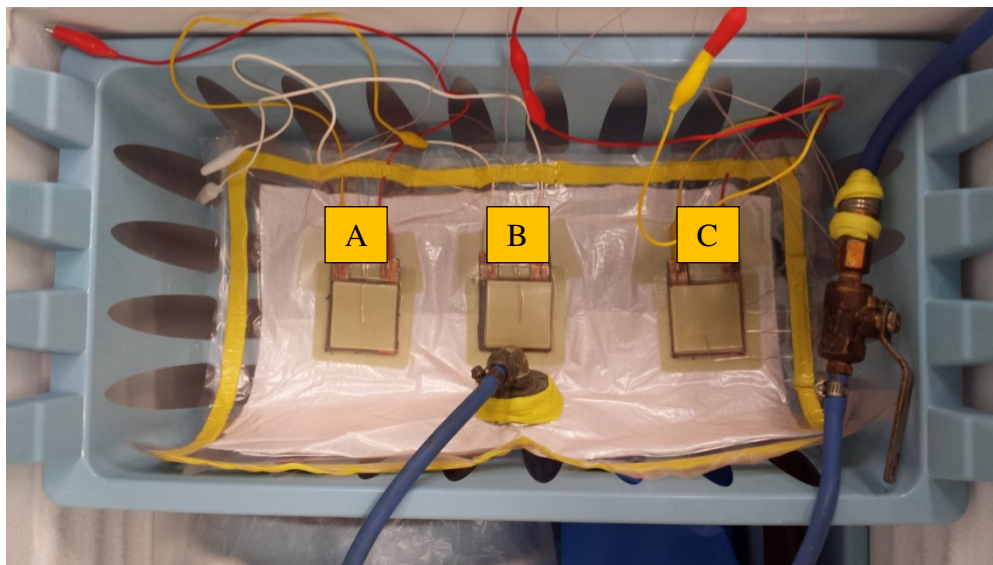


Figure 32. Prototypes set-up inside of refrigerator, A specimen is 10 layers of the carbon fabric, and B and C is 5 layers of the carbon fabric.

First attempt was applying the constant 40 volts to prototypes, but while the experiment, specimen A temperature was increased more than 430°C in 10 minutes (See Appendix C) and it burned fiberglass and vacuum bag as shown in Figure 33.

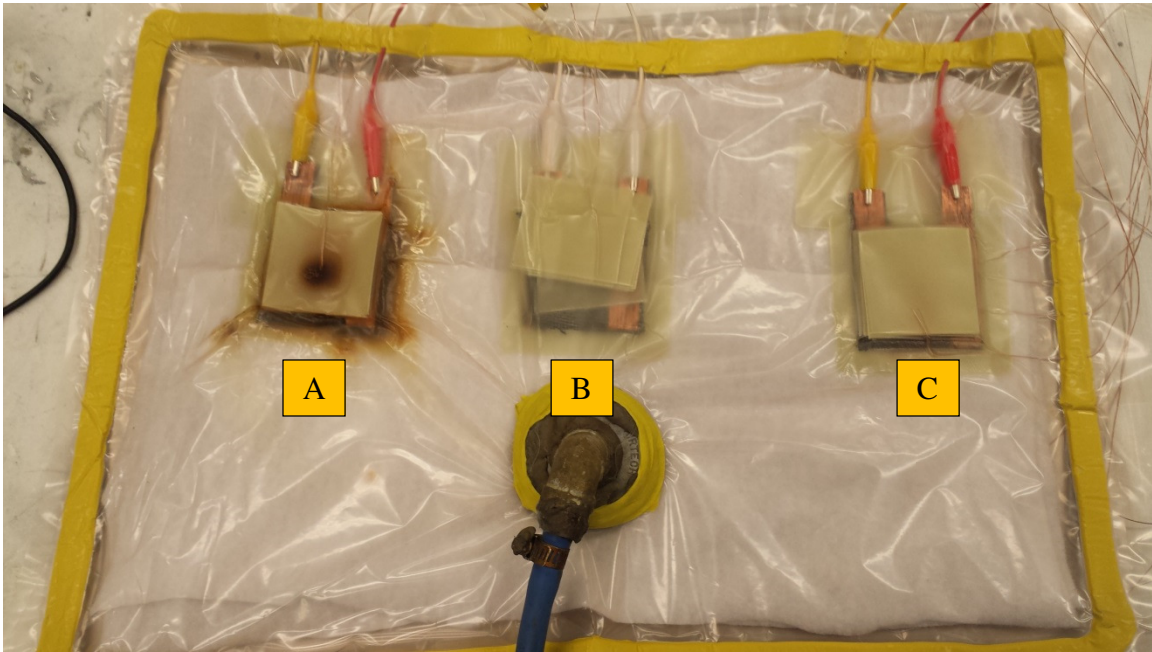


Figure 33. Burning the specimen A due to the high temperature

Vacuum bag has been damaged while the specimen A burned due to that the vacuum bag is not hold the layers of fiberglass and thermocouple as one body. Therefore in the second experiment set-up the new vacuum bag with the specimen B and C as shown in Figure 34. To decrease the maximum temperature reaches, the second experiment uses the lower voltage. But in the second trial of the experiment, the error has been occurs. The temperature reading at third layer is higher than the heat source, because thermocouple at the heat source is placed on top of the copper plate. The copper plate thermal conductivity is very high as $398 \frac{W}{m \cdot ^\circ C}$ (Chung, 2001). Therefore, the thermocouple at heat source indicated lower temperature than its actual temperature. So

the thermocouple was relocated in a different area to prevent it from touching the copper plate as shown in Figure 35.

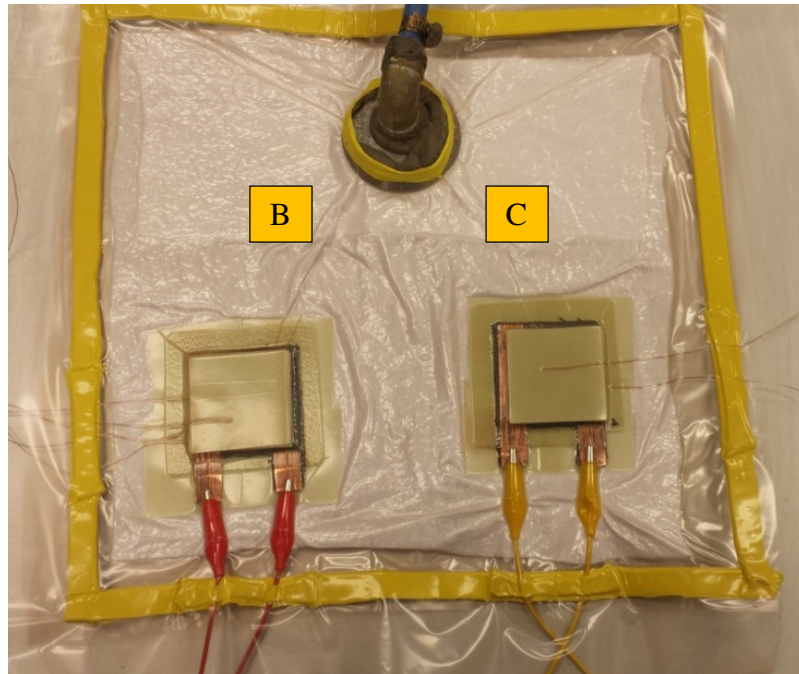


Figure 34. B and C specimens in the vacuum bag

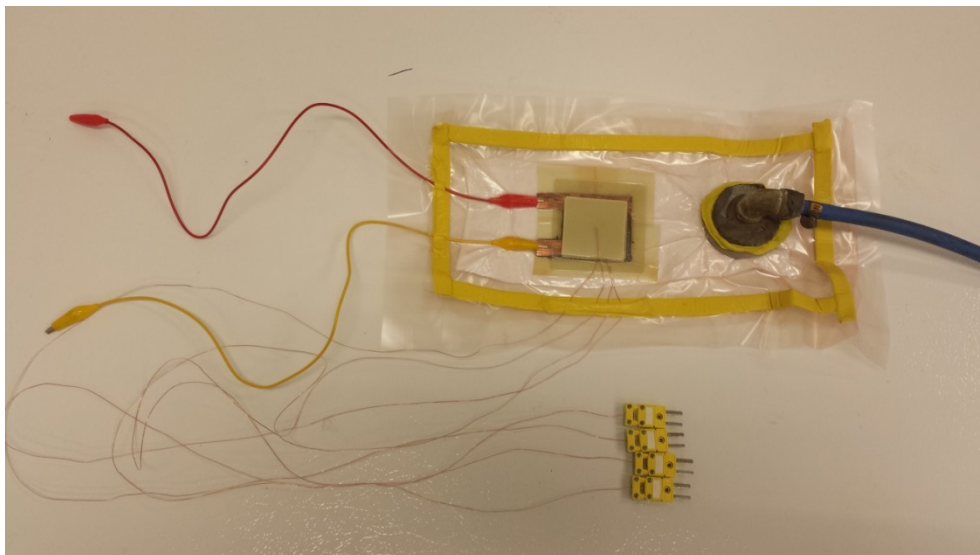


Figure 35. Single 5-layer carbon fabric specimen in the vacuum bag

With the final set-up as shown in Figure 35, three different constant voltages were applied using 20, 30, and 40 volts. During the constant 40 volts experiment applied to the five layers of carbon fabric, the fabric temperature is increased very rapidly within ten minutes that the experiment must be stopped for the safety concern. The other two voltages (20 and 30 volts) run until each of the layer temperature get into the steady state.

Chapter VI: Results and Discussion

6.1. Approximation of Resistance Equations

Most of the carbon fabric system values are unknown, such as heat capacity and resistance, because the carbon fabric system has been modified. Due to this fact, unknown resistances have to be driven by an approximation method. There are two main methods used to solve such a problem. The first method is called Beta (β) parameter method. It is used as an approximation of the characteristic of resistance that is a function of temperature. The second method is called Steinhart-Hart. It is a higher order equation to drive the resistance values. Both methods give good proximity results, but the Beta (β) parameter method gives more accurate results than the Steinhart-Hart only for the constant 20 volts.

6.1.1. Beta (β) Parameter

From the experiments, the Beta (β) and A constant can be determined. The Beta is 62.6852 K (Kelvin), and constant A is 116.702 Ω . By substituting the Beta and

constant A into Eq. 4. 4. 21, the resistance values can be determined with various temperatures as shown in Table 3.

Table 3. Beta Parameter's approximated resistance values

Resistance	Temperature (°C)
137	117.76
138	100.80
139	85.36
140	71.24
141	58.28
142	46.34
143	35.31
144	25.08
145	15.58
146	6.71
147	-1.56
148	-9.31
149	-16.58
150	-23.42

As shown in Table 3, the resistance increases with temperature decreases due to the material property of carbon. This table shows that the carbon fabric resistance values depend on the temperature. For a comparison between the theoretical values and experimental values see Figure 36.

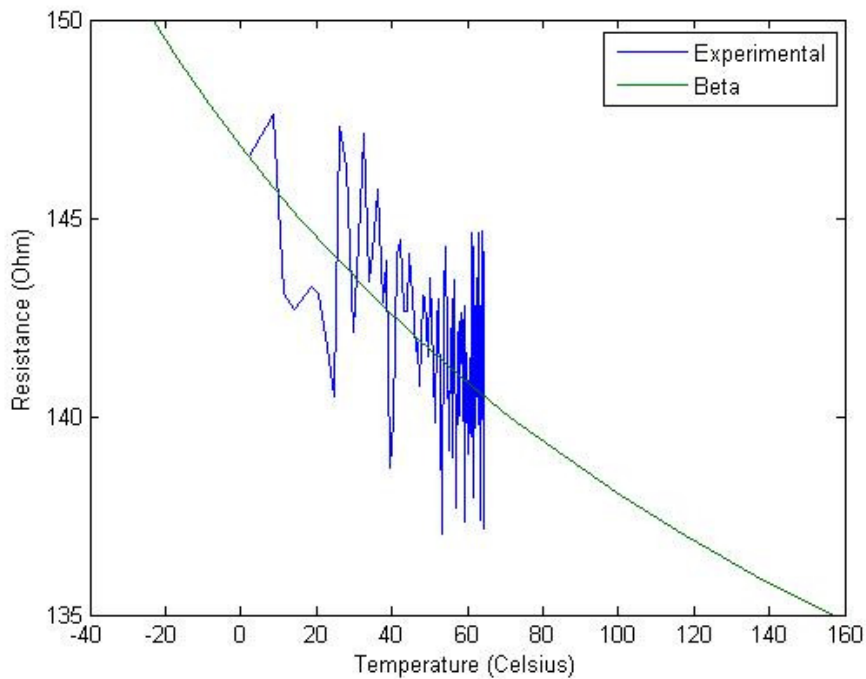


Figure 36. Comparison of resistance values between Beta Parameter and experimental

As shown in Figure 36, the Beta parameter resistance values are through the mid-section of experimental values. According to the results, the Beta parameter resistance values that function of temperature give fine proximity resistance values.

6.1.2. Steinhart-Hart

Also similar to Beta parameter, three constants (a, b, and c) can be determined from the experiment. The theoretical constants values of a, b, and c are -0.51896, 0.152294 and -0.00191. With these constants values, the approximate resistances values can be determined. Steinhart-Hart method resistance values with temperatures are shown in Table 4.

Table 4. Steinhart-Hart's approximated resistance values

Resistance	Temperature (°C)
137	97.29
138	84.48
139	72.97
140	62.58
141	53.16
142	44.61
143	36.82
144	29.71
145	23.21
146	17.24
147	11.77
148	6.74
149	2.12
150	-2.14

Also Table 4 shows negative temperature coefficient as Beta parameter. For the comparison between the theoretical Steinhart-Hart values and experimental values are shown in Figure 37. Majority, Steinhart-Hart approximation method produce higher accuracy of resistance values, but as shown in Figure 37 and Figure 38, the Beta parameter method gives more accuracy resistance values. Because the Steinhart-Hart method is third order equation, therefore, to get the accuracy value is relatively harder than the Beta parameter method for the small change in resistance. For this particular situation, using the Beta parameter method produces higher accuracy. But if the carbon fabric system generates higher temperature, it gives higher difference values in resistance, and then the Steinhart-Hart method will produce higher accuracy of resistance values.

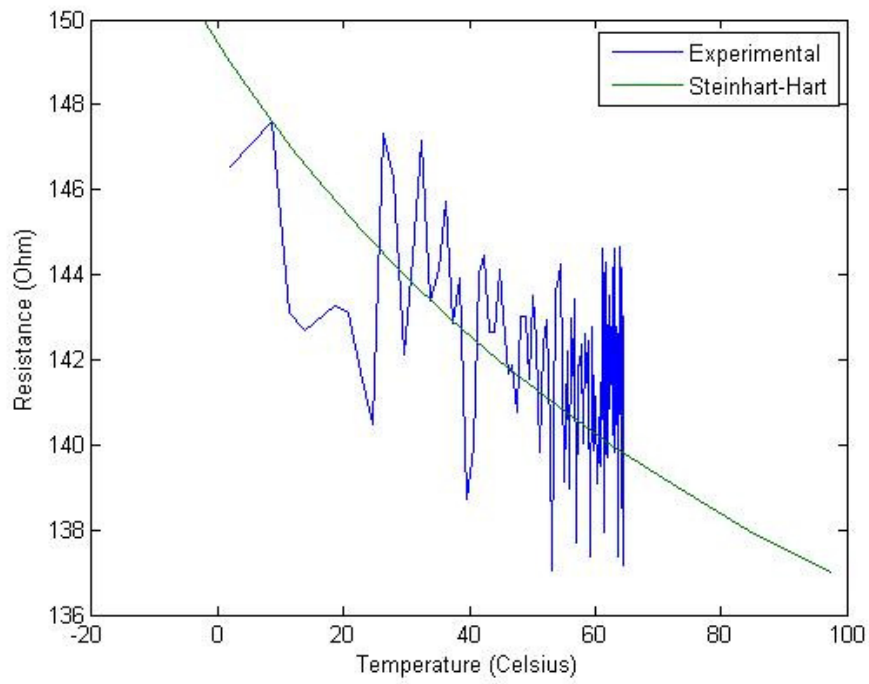


Figure 37. Comparison of resistance values between Steinhart-Hart and experimental

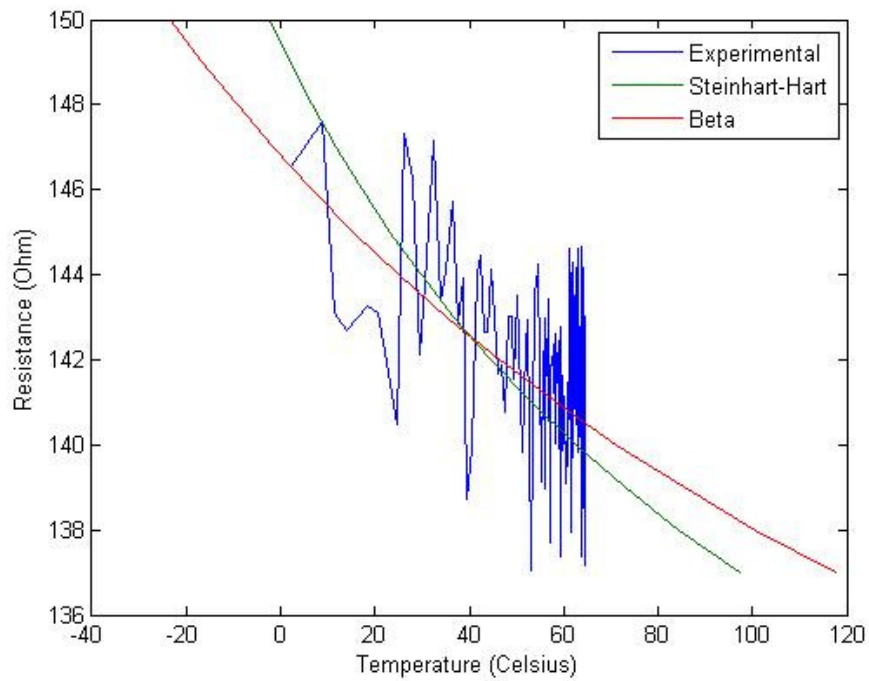


Figure 38. Comparison between both approximation method and experimental

6.2. Effect of the Negative Temperature Coefficient

Carbon is one of the common materials that have the negative temperature coefficient. The negative temperature coefficient makes resistance and temperatures are inversely proportional. In electrical system, resistance is proportional to the current, voltage, power, or thermal energy. In this paper used constant 20 voltage, which means is power or thermal energy is changing with the temperature. But for the special case as when the change in currents are small over the temperature changes, power or thermal energy can be assuming as constant.

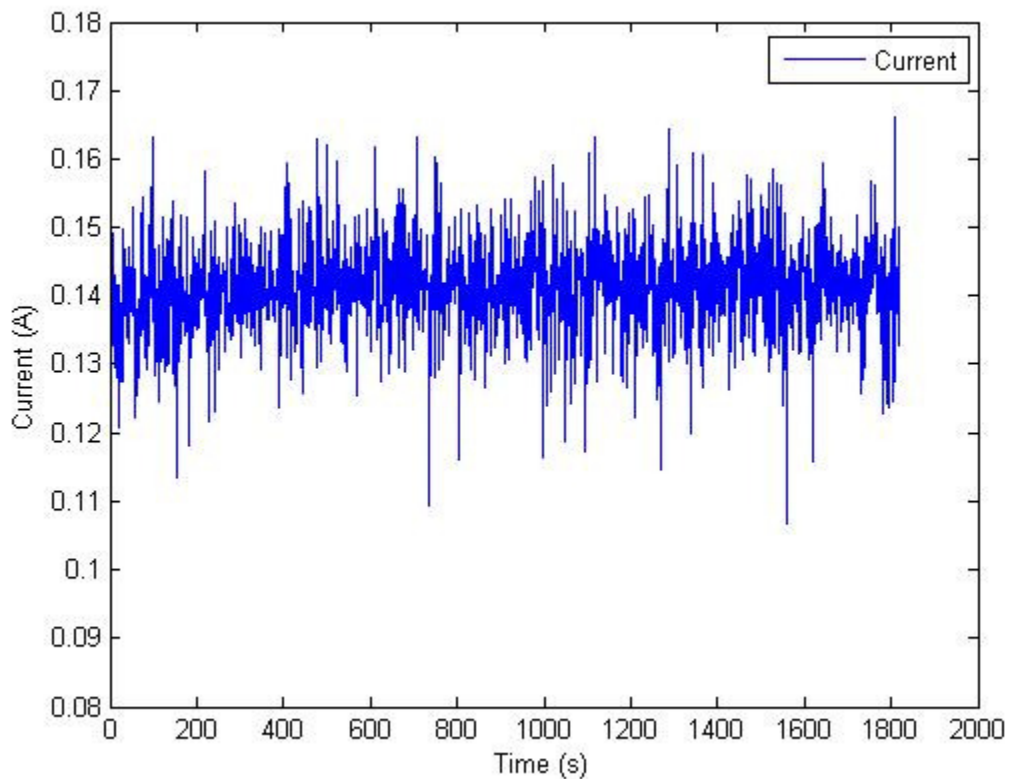


Figure 39. Experimental currents change over time

As shown in Figure 39, currents are changing very small through the time. As time passes, the temperature is changing from -14°C to 65°C (see Figure 40). In this case, current can be assuming as constant.

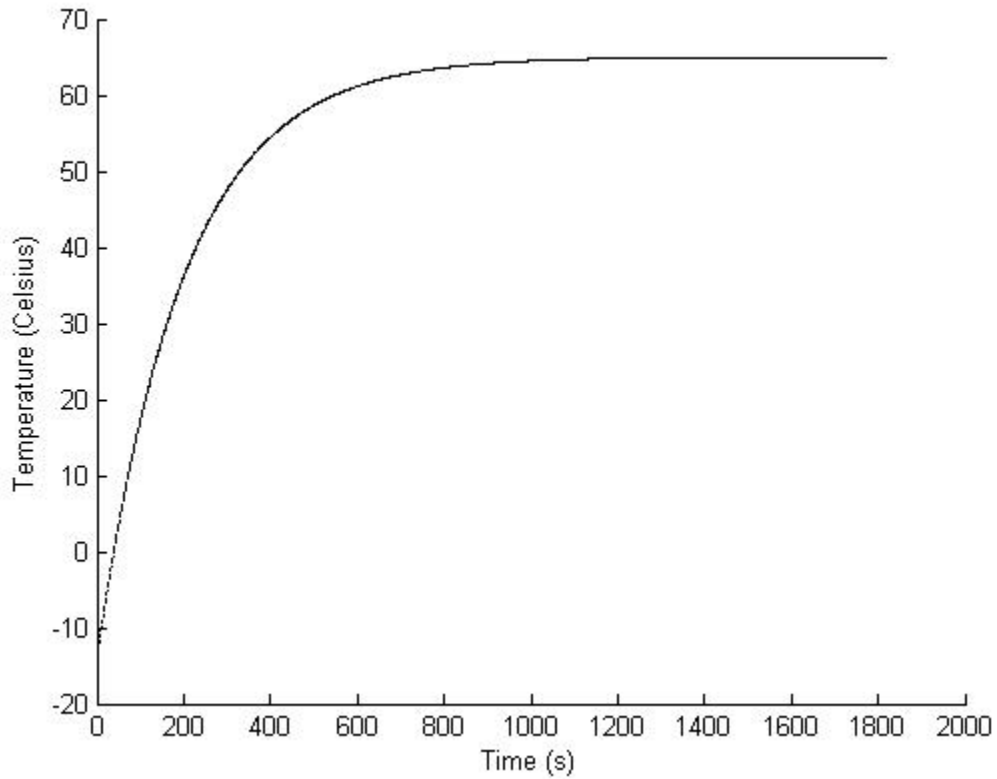


Figure 40. Theoretical temperature profile of carbon fabric

It happens due to the small resistance changing over temperature range between -14°C and 65°C . But when constant voltage increase, the temperature difference will increase. If the temperature differences are larger, it makes larger difference in resistance, so the assumption of constant current will fail. Therefore, if the voltage is lower than the constant 20 volts, the current can assume as constant.

6.3. Approximation of Heat Capacity of the Carbon Fabric System

In section 6.1 mentioned earlier, the heat capacitor is also unknown for the carbon fabric system. Therefore, it has to approximate the values by comparing the experimental values with known values.

For the heat generation of carbon fabric system, the temperature profile can be determined by using Eq. 4. 4. 16. With that temperature profile, thermal constant time can be drive with Eq. 4. 5. 3. After determine the temperature at thermal constant time of the experimental, these values are substituting into Eq. 4. 4. 12 for finding the heat capacitor.

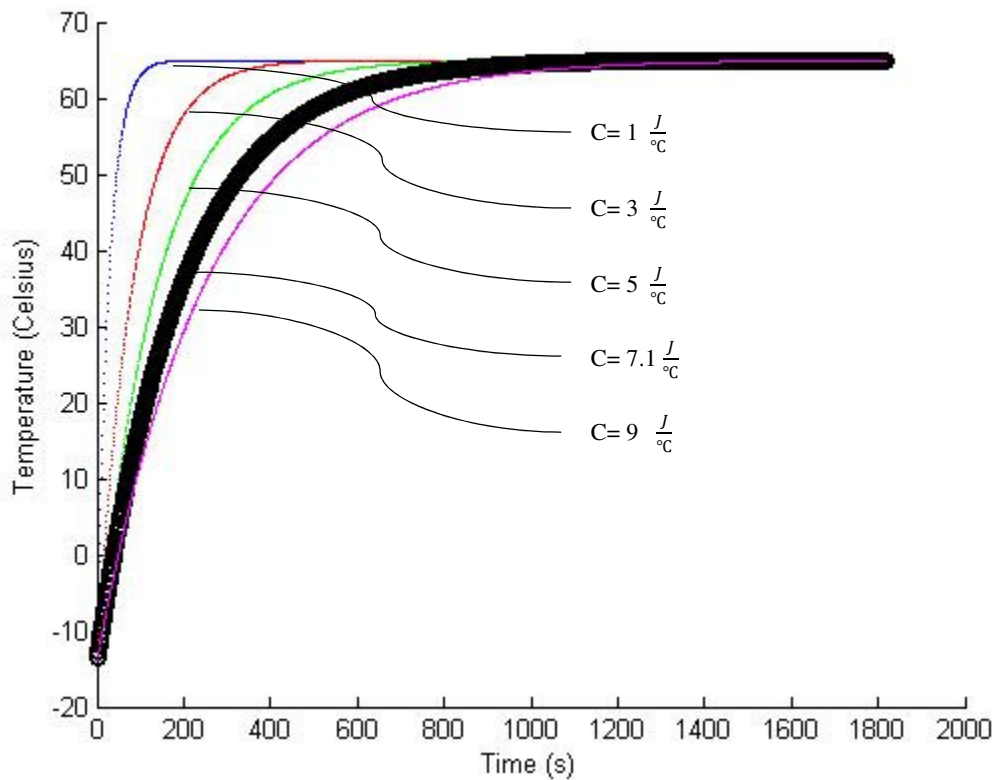


Figure 41. Effect of the temperature profile by heat capacity

6.4. Carbon Fabric Heat Generation

Within the constant voltage and current, the carbon fabric heat generation determines over the time by using the first order ordinary differential equation. While the carbon fabric generates heat, there is heat loss due to the surrounding environment. Electrical power is dissipated as heat and body of the carbon fabric temperature increase. Comparing the theoretical and experiment temperature rise depend on the time shows below figure,

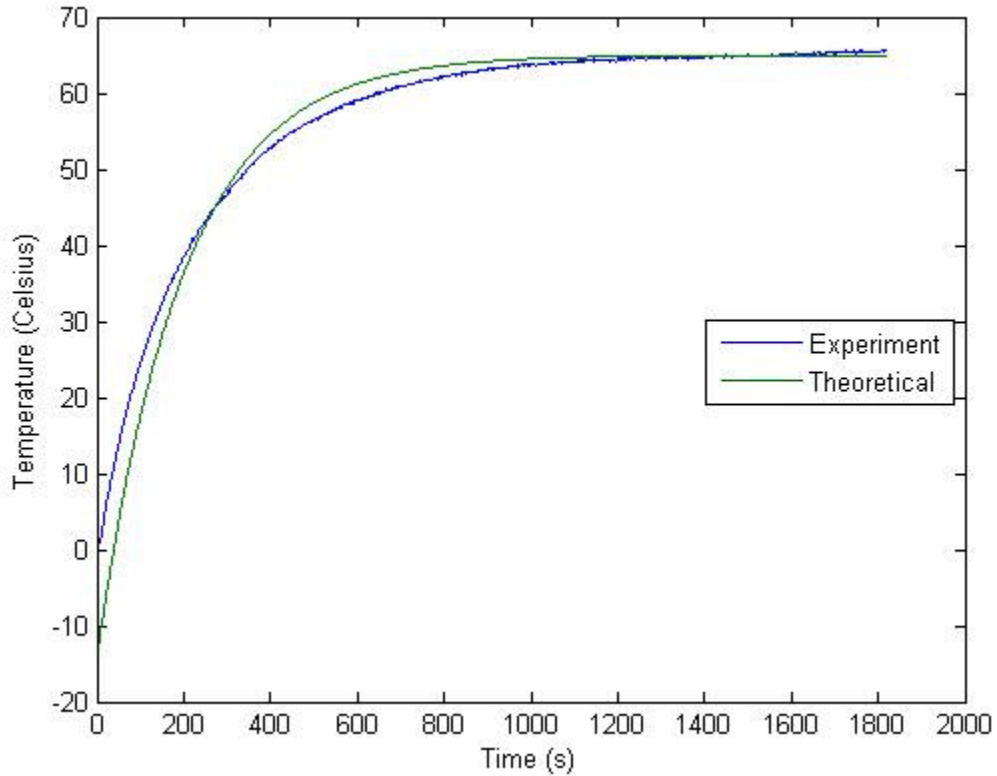


Figure 42. Comparison between experiment and theoretical carbon fabric heat generation temperature profile

Beginning portion of the experiment result indicates that the temperature starts from zero degrees Celsius. It happens due to the thermocouple signal box. This thermocouple signal box cannot measure the negative temperature. Therefore, it indicates the zero degrees Celsius. But actually, it starts from the negative temperature. Except time between zeros to 150 seconds, the percent difference of the temperature between experiment and theoretical values are less than five percent.

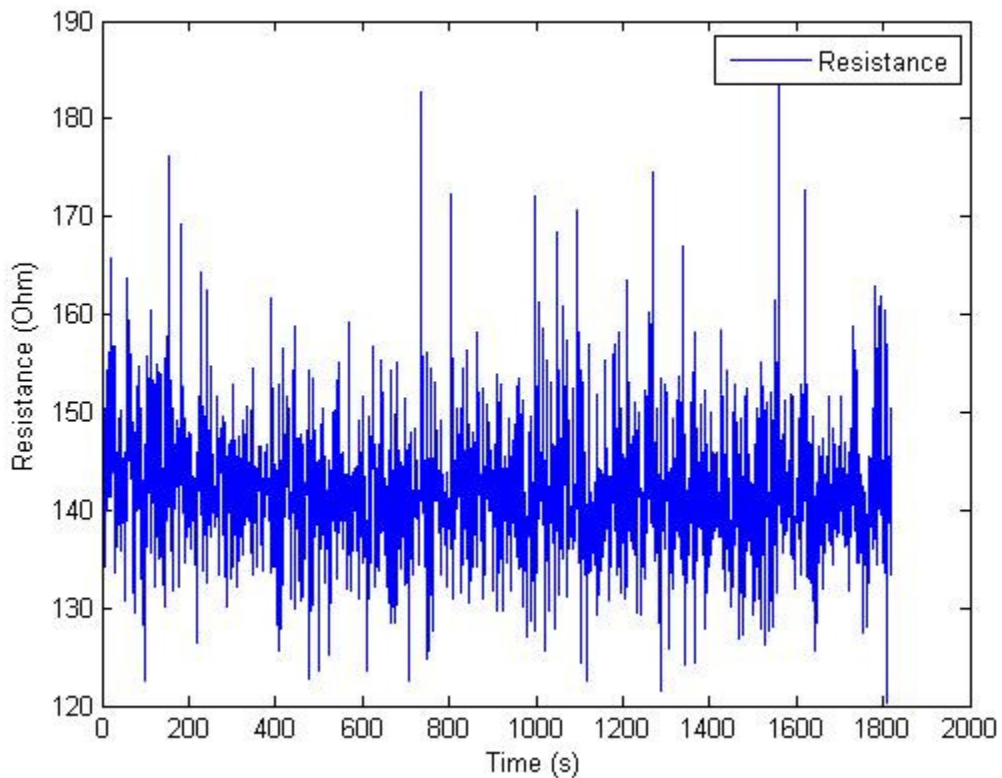


Figure 43. Resistances change over the time

The percent difference at the beginning portion came from the constant current assumption. Theoretical thermal energy at beginning portion is slightly higher than the experimental, and around 150 seconds, theoretical and experiment thermal energy become equals. As shown in Figure 43, beginning section of the resistance values are

slightly higher than the average resistance. After the beginning section, experiment temperature increase as theoretical. At the very end section, there is very small temperature difference occurs, it occurs from the pressure applied during the experiment, that causes change the resistance value.

6.5. Composite Layer Wise Temperature

According to the manufacturer, carbon fabric's raising the temperature difference over the area is less than about $\pm 2^{\circ}\text{C}$ (Hi-Carbon). It means, this system uniformly transfers the heat over the surface skin structure. In this experiment, fiberglass has been selected for the surface skin structure, because unshielded hot junction thermocouple cannot measure the temperature for the conductive material. Thermocouples are placed at the carbon fabric system, third, sixth and ninth layer of surface skin structure. The temperature rise of the each layer shows in Figure 44.

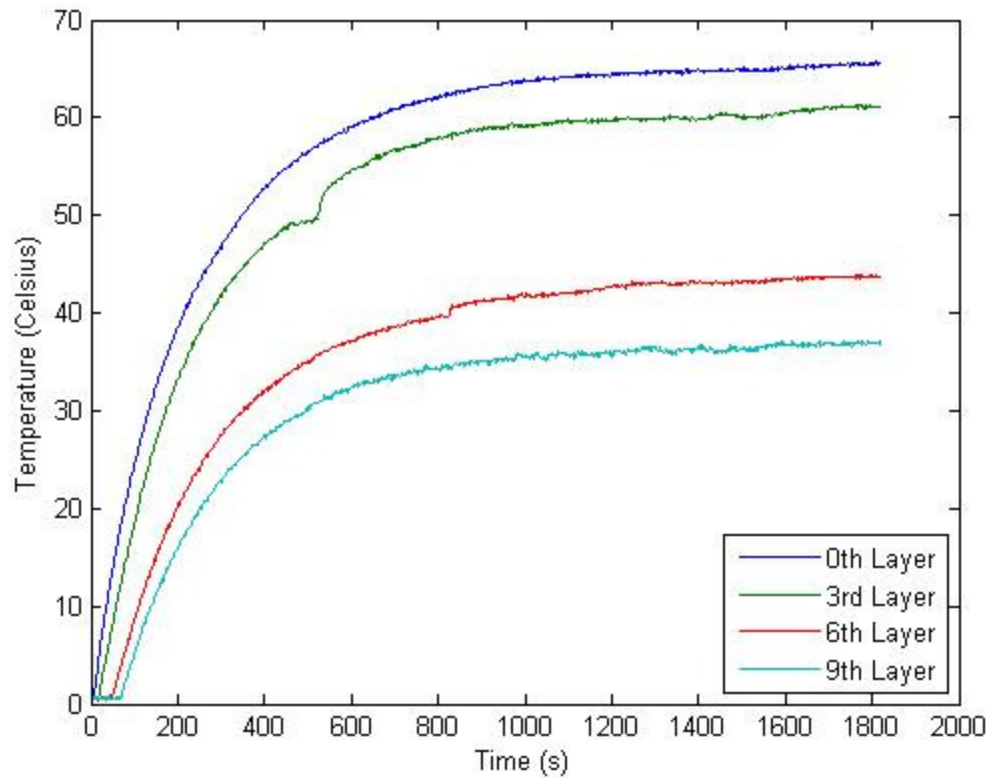


Figure 44. Temperature profiles of each layer

As mentioned at the section 6.4, the thermocouple signal box cannot measure the negative temperature. Consequently, for the ninth layer stays at near zero degrees Celsius for about 70 seconds, also at the zero layer stays at near zero degrees Celsius for several seconds. And the third layer at the temperature 50°C and the sixth layer at the temperature 40°C, temperature bumps are present. The possible causes are, these surface skins structures are not in perfect thermal contact, or the surface skin is little bit curved during the composite curing process as shown in Figure 45.

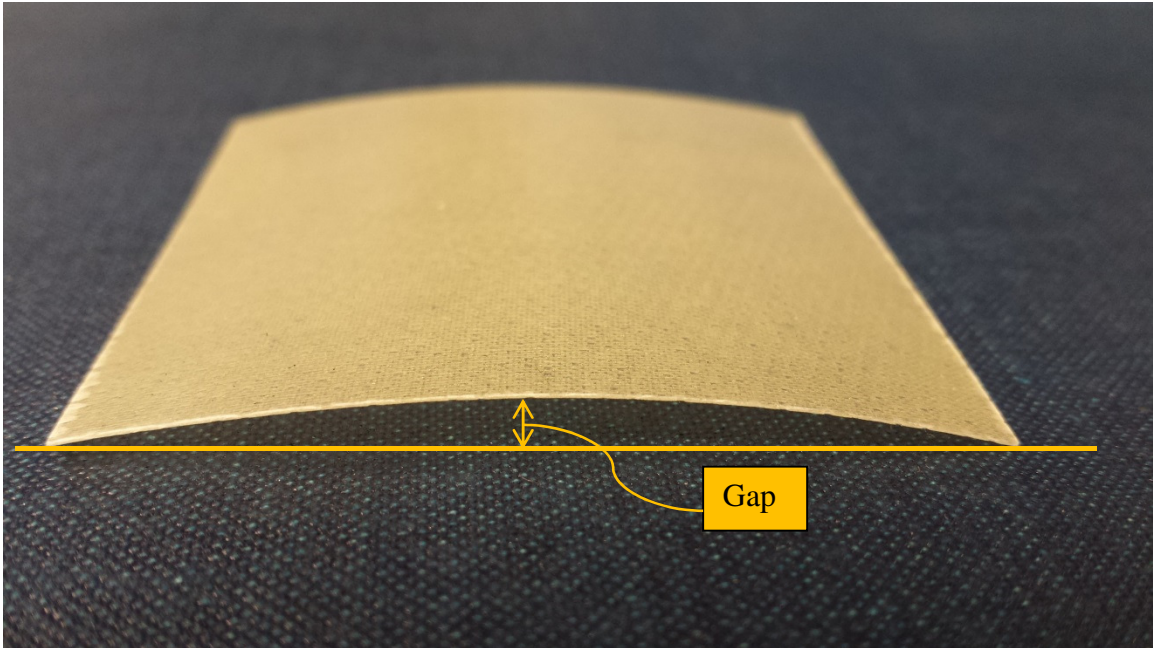


Figure 45 One Layer of the Surface Skin Structure

That curvature at the center create gap between the carbon fabric system and surface skin structure. But when the temperature increases, the gap is decreasing due to the fiberglass surface skin gets more flexible. When it gets more flexible, with the same amounts of vacuum pressure can decreasing the gap. Additionally, the thickness of the thermocouple makes more gaps. For avoid these problems, multi layers of the fiberglass have to curing with flat plate and the thermocouple wire has to be thinner.

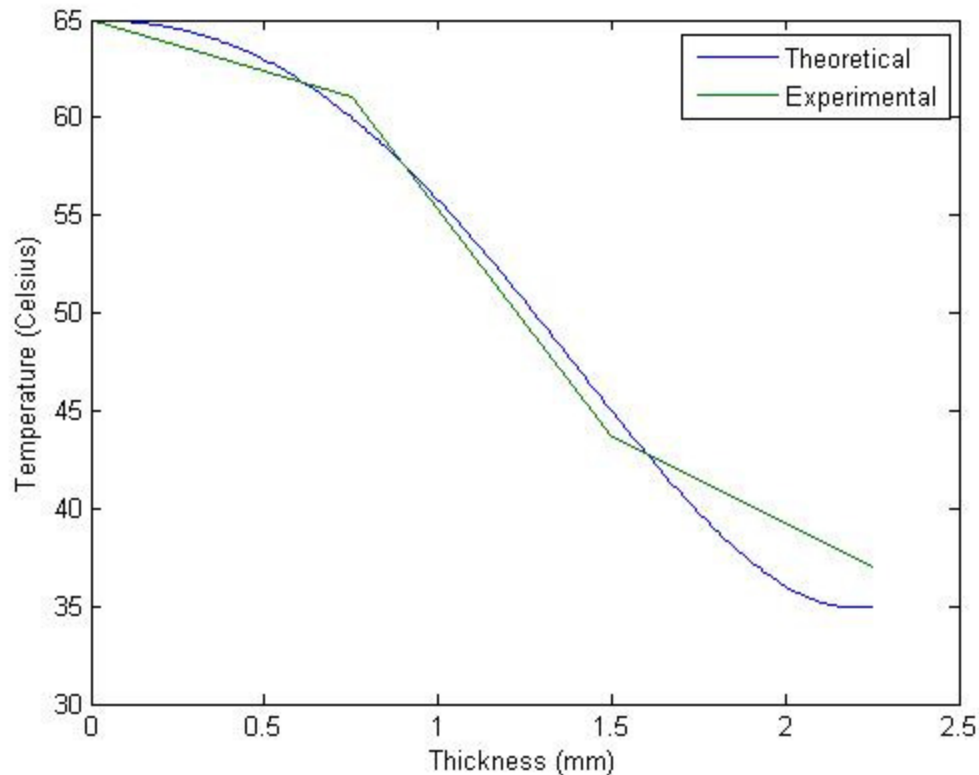


Figure 46. Comparison Temperature of layer

Fiberglass has low thermal conductivity, so compared to the metals, the quantity of heat transmitted is low. At the carbon fabric system temperature is 65°C and as shown in Figure 46, the temperature is about 35°C. There are temperature differences about 30°C between 0 layers and 9 layers. Higher the difference temperature makes more electrical power to rise the temperature.

6.6. Thermal Conductivity

Thermal conductivity is the quantity of heat transmitted through a material thickness. Higher thermal conductivity is transferring the more heat through a thickness.

Theoretically, the polymer reinforced fabric thermal conductivity can be defined. More details are explained in section 4.6.1. For the fiberglass, to determine the thermal property from other resource is difficult, because fiberglass is not commonly using in the thermal environment. Therefore, using the volume fraction, the thermal conductivity of fiberglass defined by derives the equation (Eq. 4. 7. 1 and Eq. 4. 6. 2).

Theoretical thermal conductivity is $0.084536 \frac{W}{m \cdot ^\circ C}$, and experimental thermal conductivity is $0.102673 \frac{W}{m \cdot ^\circ C}$. The percent difference is 19.38%. There are several possibilities occurs the percent difference. First, theoretical thermal conductivity used general property values. And other possible is, as the temperature increase, the thermal conductivity slightly increase. So the general case values are mostly measured at room temperature (25°C), and the experiment environment temperature is $-14^\circ C$.

As similar to the Figure 46, with same initial temperature with different thermal conductivity, it shows changing the temperature through the layers.

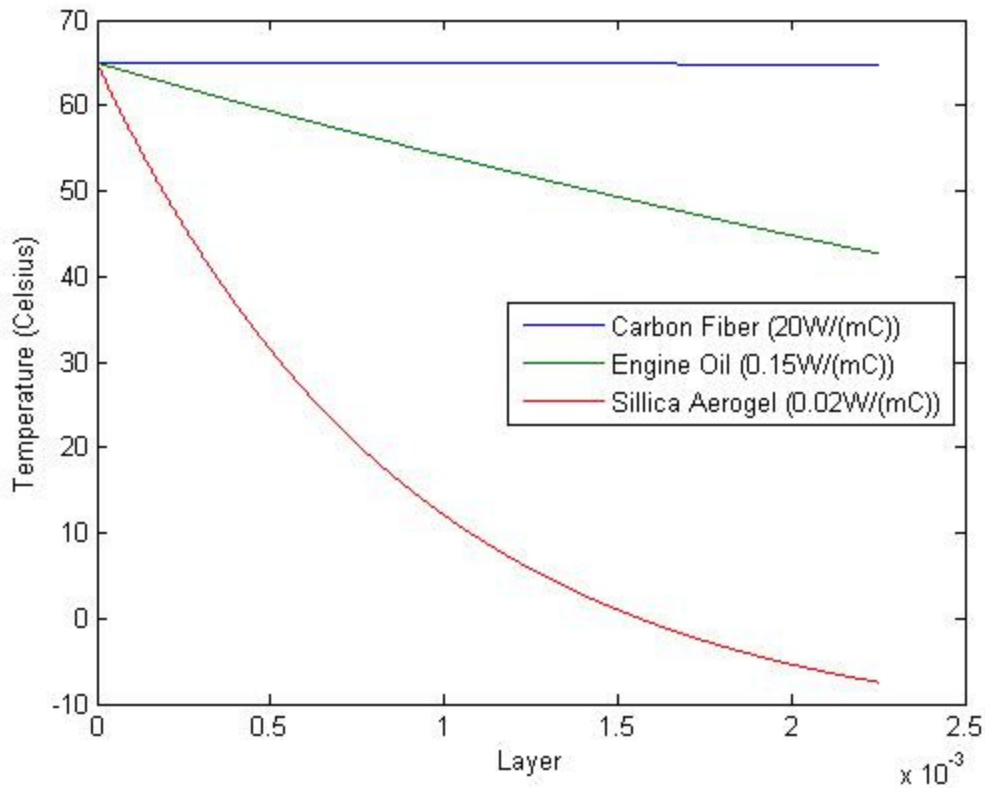


Figure 47. Comparison of the temperature with different material

Carbon fiber has high thermal conductivity, which means, there is small difference temperature between zero and ninth layer. These high conductivity materials frequently use for the heat sinks. And silica aerogel is new material that use for the thermal protection system in spacecraft. About 99.98% is air of this material; therefore, the thermal conductivity of aerogel is very similar to air. Such as, the high thermal conductivity materials can be using as heat sinks, and low thermal conductivity materials can be using as insulators.

Chapter VII: Conclusion and Future Work

7.1. Conclusion

De-icing system of an aircraft surface is one of the most necessary equipment for the weather hazards. Even if the departure place sea level temperature is high, ice can be formed on aircraft surface when an aircraft flights over the 8,000 feet from the sea level. And the weight has to be decreased for increasing efficiency of aircraft performance. Therefore in recent days, many of the aircraft manufacturer use composites materials due to their low weight. The proposed de-icing system is even about 10 times lighter than fiberglass materials. The density of this proposed de-icing system is $0.263 \frac{g}{cm^3}$.

The carbon fabric material made by woven fabrics and graphite powder thus, it is very flexible with light weight. Many of the current techniques of electrical de-icing system use the resistivity wire. It is less flexible, has a small effective area, and heavy weight. If the resistivity wire has been damaged or cut, that causes the open circuit of the electrical system which means, no heat generates due to the no current flow. In the carbon fabric system, it is designed woven fabrics types, so even if there are some

cuttings in the circuit, it will operate. And due to the material, it can attach itself to the complex curved surface. Also it can easily cover the large surface of an aircraft.

In this research experiment, fiberglass has been selected for the aircraft surface, but as shown in Figure 44, the fiberglass is not good material for wing leading edge because heat transfer from the carbon fabric to the 2.25mm thick outer surface, shows big difference in temperature. Thus, fiberglass is not a good material for the wing leading edge or control surface. As shown in Figure 47, carbon fiber is much better to use for where the de-icing system is required.

This proposed de-icing system is not instant active de-icing system as pneumatic de-icing boots, but it requires less maintenance with semi-permanent system. Also replacement wise, it can easily de-attach from the structure due to the small cell size. The operating voltage is 20 volt with direct current, therefore, it possess very safety for the electrical operation. After the power supplied, it heat up to 40°C within three minutes from the -14°C. That proves about it has high potential for using the de-icing system. With 20 volt operation voltage, it can easily predict how fast it can reach the target temperature in any temperature. Because when the supplying voltage is lower than 20 volts, the current flow is constant as mentioned in section 6.2. If the operation voltage higher than 20 volt, the operating power has to be consider the temperature, because the graphite material has temperature dependent properties.

As mentioned about the carbon material property, resistance is proportionally related with temperature. So to predict the resistance values, approximation of the characteristic of resistance methods are require. There are two main approximation method which those are Beta (β) Parameter and Steinhart-Hart methods. Most of the

time, Steinhart-Hart approximation method produces higher accurate values of resistance than Beta Parameter approximation method. But in this research, Beta Parameter method produces better results than the Steinhart-Hart method. Since Steinhart-Hart method is higher order equation, the small change in the resistance values will produce a higher error than the Beta Parameter method. But if the operation voltage is higher than the 30 volt, the Beta parameter method will produce higher error.

The theoretically calculated thermal conductivity of the fiberglass has some percentage difference with the experiment. The percentage difference might come from using the typical properties of fiberglass. If using the right properties of this fiberglass, it will cause the lower the percent difference.

Carbon fabric de-icing system improved some disadvantages from the current techniques as weight, heating area, and replacement. And it also gives satisfied results for the temperature incensement. Finally, the heat flux for the carbon fabric system is $0.11272 \frac{W}{cm^2}$ and that heat flux produces maximum temperature around $67^{\circ}C$.

7.2. Future Work

Numerical analysis of the proposed de-icing system with the temperature dependence thermal conductivity has to be simulated. A flat plate structure is examined in this research and curved structures with a thick plate can be examined in future. One recommendation is using the pure carbon fiber as heat source. When it was tested for few times, the carbon fibers generated more heat in much shorter time. If pure carbon fibers can be controlled, it would make a better de-icing system compared to the fabrics.

References

- Abbey, T. (2014, October 1). *FEA and Composites, Part 1*. Retrieved from Desktop Engineering: <http://www.deskeng.com/de/fea-composites-part-1/>
- Antonopoulos, K., & Tzivanidis, C. (1995). Analytical solution of boundary value problems of heat conduction in composite regions with arbitrary convection boundary conditions. *ACTA Mechanica*.
- Arnal, C., Alzueta, M., Millera, A., & Bibao, R. (2011, September 11). Experimental And kinetic Study of the Interaction of a Commercial Soot Toward NO at High Temperature. *University of Zaragoza*. Cagliari, Sardinia, Italy.
- BEA. (2012). Final Report On the accident on 1st June 2009 to the Airbus A330-203 registered F-GZCP operated by Air France flight AF 447 Rio de Janeiro - Paris. *Bureau d'Enquetes et d'Analyses*.
- Bhat, N., Seshadri, D., Nate, M., & Gore, A. (2006). Development of conductive cotton fabrics for heating devices. *Journal of Applied Polymer Science, Vol. 102*, 4690-4695.
- Buck, R. (2004, October). Aircraft Deicing and Anti-icing Equipment. *AOPA Air Safety Foundation*. (K. D. Murphy, & L. Bell, Eds.) Frederick, Maryland, USA: Bruce Landsberg.
- Cahalin. (2011, December). *Thermawing Aircraft Deicing system*. Retrieved from Kelly Aerospace: <http://www.kellyaerospace.com/thermawing-aircraft-deice.html#>
- Callister, J. (2003). *Materials science and engineering an introduction*. John Wiley & Sons, Inc.
- Campbell, F. (2010). Introduction to Composite Materials. *ASM International*.
- Cheng, K., & Fujii, T. (2007). *Heat Transfer Engineering*. April: 27.

- Chung, D. (2001). Materials for thermal conduction. *Applied thermal engineering* 21, 1593-1605.
- Committee, I. A. (2013). Final Report On Results of Investigation of Accident . *Interstate Aviation Committee Air Accident Investigation Commission*.
- Conrad, L. (2010, April). *Weather*. Retrieved from NASA:
<http://virtualskies.arc.nasa.gov/weather/4.html>
- Dillingham, G. (2010). Preliminary Information on Aircraft Icing and Winter Operations. *United States Government Accountability Office*.
- Duchon, R. (2010, September 26). Remedies to Prevent Plane Crashes Languish. *News21*. Retrieved December 22, 2014, from <http://national.news21.com/2010-2/plane-crashes-avoidable-with-safety-measures-ntsb/6/index.html>
- Evans, D. (1988). Wing Ice Hinted In B-1b Crash. *Chicago Tribune*.
- Falzon, B., Robinson, P., Frenz, S., & Gilbert, B. (2015). Development and evaluation of a novel integrated anti-icing/de-icing technology for carbon fibre composite aerostructures using an eletro-conductive textile. *Composites: Part A* 68, 323-335.
- Flight Safety*. (n.d.). Retrieved from Pilotfriend:
http://www.pilotfriend.com/safe/safety/icing_conditions.htm
- Forced & Natural Convection*. (n.d.). Retrieved December 23, 2014, from EESA:
<http://www.spaceflight.esa.int/impress/text/education/Heat%20Transfer/Convection%2002.html>
- Fosbury, A., Wang, S., Pin, Y., & Chung, D. (2003). The interlaminar interface of a carbon fiber polymer-matrix composite as a resistance heating element. *Composites: Part A* 34, 933-940.
- Freed, J. (2013). GE readies fix for engine icing on 787s, 787-8s. *The Seattle Times*.

- Grantz, M. (2012, May 02). *Heavy ice accumulation on aircraft surfaces 3*. Retrieved from Deicing Training: http://training.deicinginnovations.com/?attachment_id=1579
- HiCARBON. (2011). Retrieved from Hi-Carbon: <http://hi-carbon.com/#page>
- Hi-Carbon. (n.d.). *Hi-Carbon*. Retrieved from Pogunhan saesang inc.: www.epogni.com/sc_2_1_1.php
- Hisashi, H., Arata, S., & Sekine, Y. (2002, April 16). High-Resistivity Carbon Black. *US 6,372,349 B1*. United States Patent.
- Holman, J. (2010). *Heat Transfer Tenth Edition*. New York, NY: McGraw Hill.
- Hradecky, S. (2011). Crash: Sol SF34 near Los Menucos on May 18th 2011, severe icing, stall, loss of control. *The Aviation Herald*.
- Hudson, J. (1992). Technical Manual Aviation Unit Maintenance and Aviation intermediate Maintenance Manual for General Aircraft Maintenance (Electrical and Instrument Maintenance Procedures and Practices) Volume 4. *Headquarters Department of The Army*.
- Johnson, T. (2015). *History of Composites*. Retrieved from About money: <http://composite.about.com/od/aboutcompositesplastics/a/HistoryofComposites.htm>
- Kim, T., & Chung, D. (2003). Carbon fiber mats as resistive heating elements. *Carbon Volume 41, Issue 12*, 2436-2440.
- Lee, S. M. (1989). *Dictionary of Composite Materials Technology*. Lancaster, Pennsylvania: Technomic.
- Millikan, R. A., & Bishop, E. S. (1917). *Elements of Electricity: A Practical Discussion of the Fundamental Laws and Phenomena of Electricity and Their Practical Applications in the Business and Industrial World*. Chicago: American Technical Society.

- Moran, M., Shapiro, H., Boettner, D., & Bailey, M. (2011). *Fundamentals of Engineering Thermodynamics 7th Edition*. Hoboken: John Wiley & Sons, Inc.
- Nadel, B. A. (2006, June). *Fiberglass Fenestration: A Durable, Sustainable, and Economic Alternative for Windows and Doors*. Retrieved November 27, 2014, from NE Fiberglass Windows:
<http://www.newenglandfiberglasswindows.com/fiberglassfenestration.html>
- NI Corp. (n.d.). *SCB-100*. Retrieved from National Instruments:
<http://sine.ni.com/nips/cds/view/p/lang/en/nid/1181>
- Oechsner, A., & Murch, G. (2011). *Heat Transfer in Multi-Phase Materials*. Springer.
- Ozisik, M. (1968). *Boundary Value Problems of Heat Conduction*. Scranton, PA: International Textbook Company.
- Prucnal, D. (2013, November 1). *Doing more with less: Cooling computers with oil pays off*. Retrieved from National Security Agency:
<https://www.nsa.gov/research/tnw/tnw202/article4.shtml>
- Rolfes, R. (1990). Efficient Thermal Analysis of Anisotropic Composite Plates Using New Finite Elements. *Developments in the Science and Technology of Composite Materials*, 743-748.
- Shenai-Khatkhate, D. V. (2013, April 18). *Neoprene was invented 83 years ago, on April 17, 1930*. Retrieved November 26, 2014, from Deo Volente:
<https://dshenai.wordpress.com/2013/04/18/neoprene-was-invented-83-years-ago-on-april-17-1930/>
- Steuernagle, J., Roy, K., & Wright, D. (2002). Aircraft Icing. *AOPA Air Safety Foundation*, 1-16.
- Subrenat, A., & Cloirec, P. (2003). Thermal behavior of activated carbon cloths heated by Joule effect. *Journal of environmental engineering*, 1077-1084.

- Tavman, I., & Akinci, H. (2000). Transverse thermal conductivity of fiber reinforced polymer composites. *International Communications in heat and Mass Transfer*, 253-261.
- Thermal Time Constant*. (2012, May 25). Retrieved from U.S.Sensor Corp.:
<http://www.ussensor.com/thermal-time-constant>
- TKS. (2012, May 31). *Weeping Wings*. Retrieved from Bonanza Install Part 5:
<https://weepingwings.wordpress.com/tag/tks/>
- Tobias, S., & Koenigsberger, F. (1970). *Advances in Machine Tool Design and Research 1969. Proceedings of the 10th international M.T.D.R. Conference*. Pergamon Press.
- Tsymbol, E. (2005). Section 5: Lattice Vibrations.
- University, T. (2002, September 4). *Gourmet Engineering*. Retrieved from Chapter 1:
Overview of Heat Transfer:
http://www.tufts.edu/as/tampl/en43/lecture_notes/ch1.html
- Weather*. (n.d.). Retrieved from National Aeronautics and Space Administration:
<http://virtualskies.arc.nasa.gov/weather/4.html>
- Wikipedia. (2015, March 12). *Carbon black*. Retrieved from Wikipedia:
http://en.wikipedia.org/wiki/Carbon_black
- Wong, C., Ambrosi, A., & Pumera, M. (2012, August 21). Thermally reduced graphenes exhibiting a close relationship to amorphous carbon. *DOI:10.1039/c2nr30989k*.
- Zimmer, M., Fan, X., Bao, J., Liang, R., Wang, B., Zhang, C., & Brooks, J. (2012). Through-thickness thermal conductivity prediction study on Nanocomposites and multiscale composites. *Materials Sciences and Applications*, 131-138.

Appendix A: 5 Layers of carbon fabric with 30 VDC

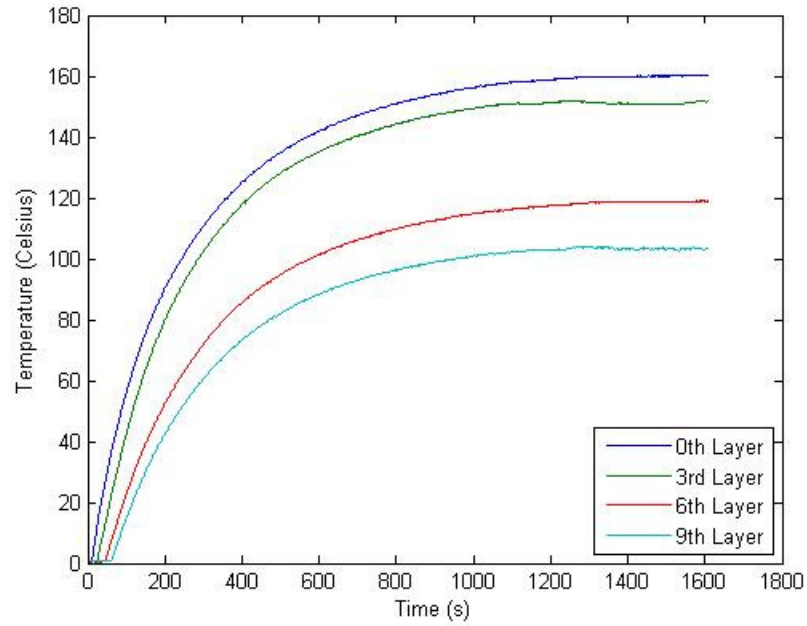


Figure 48. Temperature profile for 30 VDC

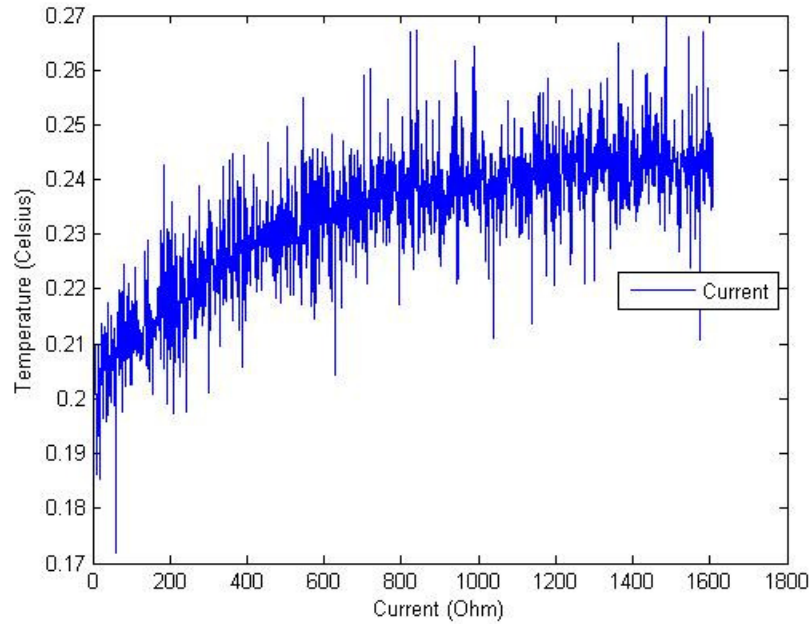


Figure 49. Current profile for 30 VDC

Appendix B: 5 Layers of carbon fabric with 40 VDC

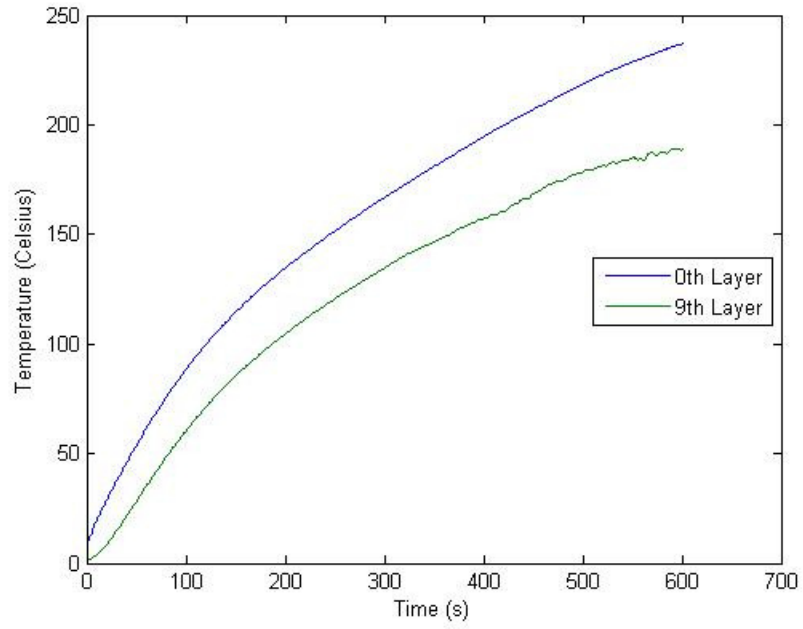


Figure 50. Temperature profile for 40 VDC

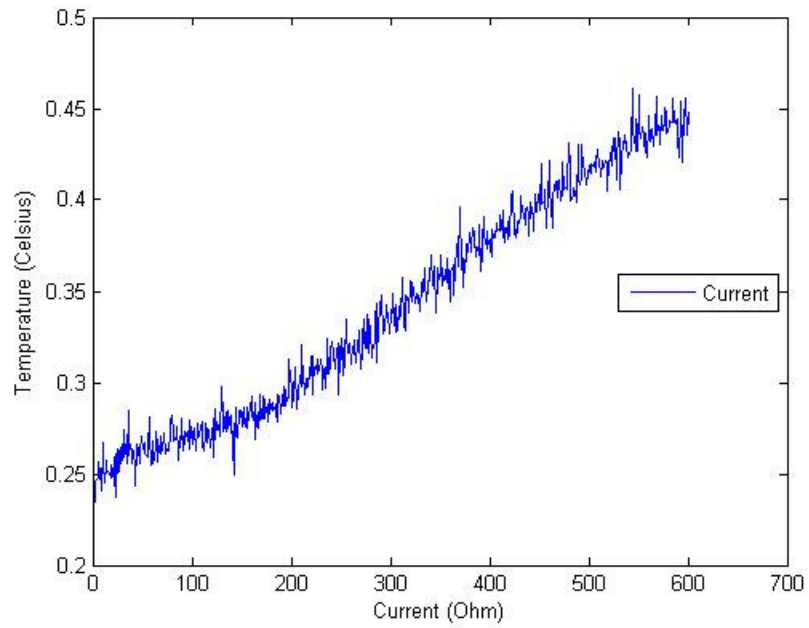


Figure 51. Current profile for 40 VDC

Appendix C: 10 Layers of carbon fabric with 40 VDC

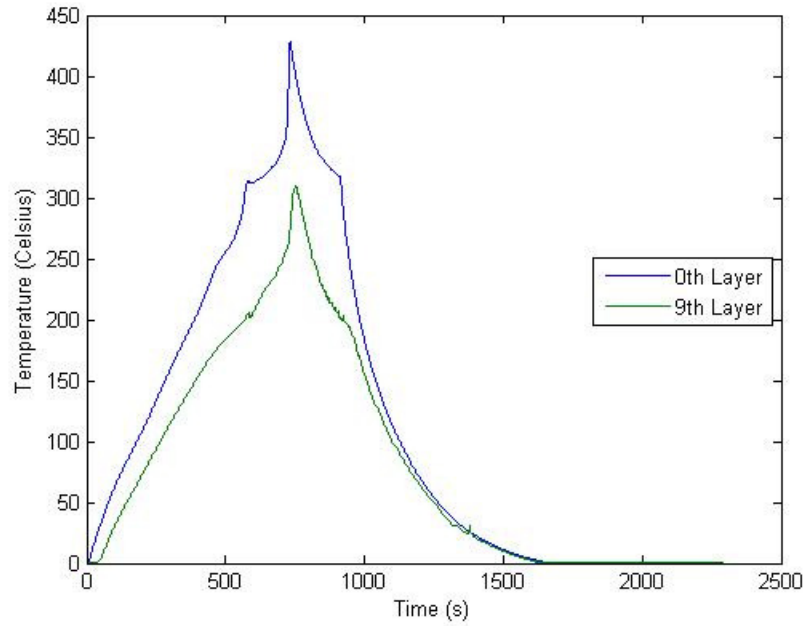


Figure 52. 10 Layers of carbon fabric temperature profile for 40 VDC, around 800s, carbon fabric burned fiberglass

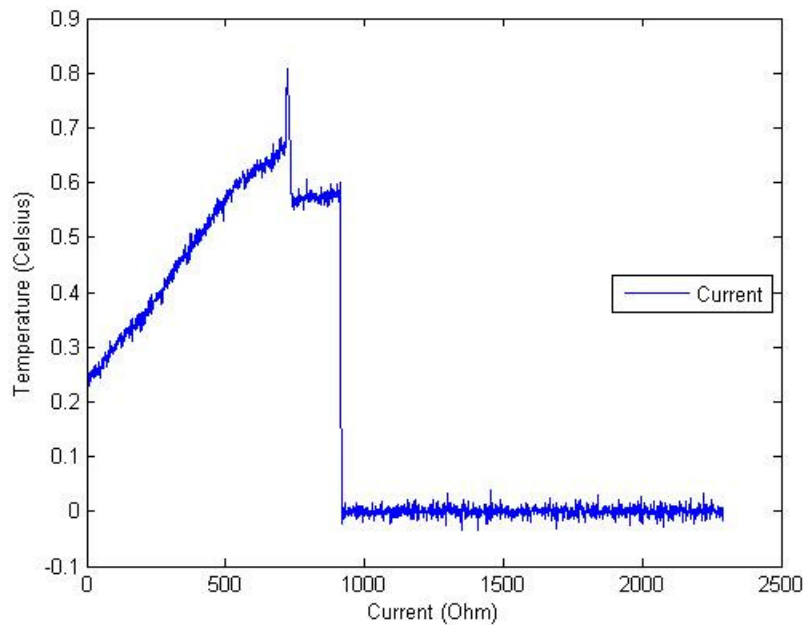


Figure 53. 10 Layers of carbon fabric current profile for 40 VDC, around the 900s turned power off